



# An NT-3-releasing bioscaffold supports the formation of *TrkC*-modified neural stem cell-derived neural network tissue with efficacy in repairing spinal cord injury

Ge Li<sup>a,b,c,d</sup>, Bao Zhang<sup>c</sup>, Jia-hui Sun<sup>a</sup>, Li-yang Shi<sup>e</sup>, Meng-yao Huang<sup>g</sup>, Li-jun Huang<sup>c</sup>, Zi-jing Lin<sup>c</sup>, Qiong-yu Lin<sup>b</sup>, Bi-qin Lai<sup>a,c,d,f</sup>, Yuan-huan Ma<sup>a,c,d</sup>, Bin Jiang<sup>g</sup>, Ying Ding<sup>c,d</sup>, Hong-bo Zhang<sup>c</sup>, Miao-xin Li<sup>h</sup>, Ping Zhu<sup>b</sup>, Ya-qiong Wang<sup>i</sup>, Xiang Zeng<sup>a,c,d,\*\*</sup>, Yuan-shan Zeng<sup>a,c,d,f,g,\*</sup>

<sup>a</sup> Key Laboratory for Stem Cells and Tissue Engineering, Ministry of Education, Sun Yat-sen University, Guangzhou, 510080, China

<sup>b</sup> Guangdong Cardiovascular Institute, Guangdong Provincial People's Hospital, Guangdong Academy of Medical Sciences, Guangzhou, Guangdong, 510100, China

<sup>c</sup> Department of Histology and Embryology, Zhongshan School of Medicine, Sun Yat-sen University, Guangzhou, 510080, China

<sup>d</sup> Institute of Spinal Cord Injury, Sun Yat-sen University, Guangzhou, 510120, China

<sup>e</sup> State Key Laboratory of Chemo/Biosensing and Chemometrics, College of Biology, Hunan University, Changsha, 410082, China

<sup>f</sup> Co-innovation Center of Neuroregeneration, Nantong University, Nantong, 226001, China

<sup>g</sup> Guangdong Provincial Key Laboratory of Brain Function and Disease, Zhongshan School of Medicine, Sun Yat-sen University, Guangzhou, 510080, China

<sup>h</sup> Laboratory of Precision Medical Genomics, Zhongshan School of Medicine, Sun Yat-sen University, Guangzhou, 510080, China

<sup>i</sup> Department of Electron Microscope, Zhongshan School of Medicine, Sun Yat-sen University, Guangzhou, 510080, China

## ARTICLE INFO

### Keywords:

Neurotrophin-3  
Tropomyosin kinase receptor C  
Self-organization  
Neural network tissue  
Spinal cord injury

## ABSTRACT

The mechanism underlying neurogenesis during embryonic spinal cord development involves a specific ligand/receptor interaction, which may be help guide neuroengineering to boost stem cell-based neural regeneration for the structural and functional repair of spinal cord injury. Herein, we hypothesized that supplying spinal cord defects with an exogenous neural network in the NT-3/fibroin-coated gelatin sponge (NF-GS) scaffold might improve tissue repair efficacy. To test this, we engineered *tropomyosin receptor kinase C (TrkC)*-modified neural stem cell (NSC)-derived neural network tissue with robust viability within an NF-GS scaffold. When NSCs were genetically modified to overexpress *TrkC*, the NT-3 receptor, a functional neuronal population dominated the neural network tissue. The pro-regenerative niche allowed the long-term survival and phenotypic maintenance of the donor neural network tissue for up to 8 weeks in the injured spinal cord. Additionally, host nerve fibers regenerated into the graft, making synaptic connections with the donor neurons. Accordingly, motor function recovery was significantly improved in rats with spinal cord injury (SCI) that received *TrkC*-modified NSC-derived neural network tissue transplantation. Together, the results suggested that transplantation of the neural network tissue formed in the 3D bioactive scaffold may represent a valuable approach to study and develop therapies for SCI.

## 1. Introduction

Severe trauma to the spinal cord can lead to sensorimotor disorders, or even permanent paralysis [1]. A hostile post-injury

microenvironment (consisting of chronic inflammation, glial scarring, and cavity formation) with a reduced regenerative capacity (neuronal loss) can disrupt the continuity of signal transmission between the brain and the limbs and hinder functional recovery after severe spinal cord

Peer review under responsibility of KeAi Communications Co., Ltd.

\* Corresponding author. Department of Histology and Embryology, Zhongshan School of Medicine, Sun Yat-sen University, 74# Zhongshan 2nd Road, Guangzhou, 510080, China.

\*\* Corresponding author. Department of Histology and Embryology, Zhongshan School of Medicine, Sun Yat-sen University, 74# Zhongshan 2nd Road, Guangzhou, 510080, China.

E-mail addresses: [zengx33@mail.sysu.edu.cn](mailto:zengx33@mail.sysu.edu.cn) (X. Zeng), [zengysh@mail.sysu.edu.cn](mailto:zengysh@mail.sysu.edu.cn) (Y.-s. Zeng).

<https://doi.org/10.1016/j.bioactmat.2021.03.036>

Received 1 December 2020; Received in revised form 3 March 2021; Accepted 18 March 2021

2452-199X/© 2021 The Authors. Publishing services by Elsevier B.V. on behalf of KeAi Communications Co. Ltd. This is an open access article under the CC

BY-NC-ND license (<http://creativecommons.org/licenses/by-nc-nd/4.0/>).

injury [2]. Thus, it is essential to improve the microenvironment and concurrently replenish damaged neurons that can form new relay circuits to replace the ruptured ones. Several studies have reported that the provision of trophic factors can create a pro-regenerative microenvironment, thereby boosting endogenous repair in both rats and nonhuman primates with SCI [3–5]. We have previously devised an NT-3-controlled releasing scaffold, in which NT-3 is encapsulated within a fibroin fibril linked to a gelatin sponge (GS) scaffold [6]. We showed that GS exhibited good cytocompatibility, histocompatibility, and low toxicity, suggesting that it may have clinical translational value. A porous structure and soft mechanical property allow it to act as an innocuous underprop, inhibiting the seeded cells from migrating in the direction of flow of the cerebrospinal fluid, and constitutes an excellent candidate material to mimic the solid structure of the spinal cord. When the scaffold was grafted into an injured spinal cord, we observed a persistent release of NT-3 along with fibroin degradation in the post-injury environment. Furthermore, we found newly born neurons in the graft/injury area in response to NT-3 release. However, the overall endogenous neuronal population in the scaffold was inadequate, and led to only a modest functional improvement [7]. Although improvements can be made to fine-tune the design of materials aiming to boost endogenous neurogenesis, the reinnervation of the injury area can also be increased through the transplantation of exogenous neurons. Grafted neural stem/progenitor cells (NSCs/NPCs) can differentiate into functional neurons when they are loaded into scaffolds together with multiple trophic factors [8,9]. However, it remains to be determined whether the microenvironment established by the continual release of a single trophic factor can support the survival of a large number of donor neurons grafted into the lesion site.

The potential of NSCs to differentiate into neurons renders them an ideal source of seed cells for the treatment of neurological diseases [10]. However, their therapeutic efficacy is limited by their propensity to differentiate into astroglia rather than neurons in the inhibitory milieu of the injured spinal cord, highlighting the need to provide a microenvironment that encourages the neuronal differentiation of the grafted stem cells. The sustained release of neurotrophic factors or drugs, which is believed to contribute to stem cell safety and promote their neuronal differentiation [11], would represent an effective strategy to harness a donor NSC-derived neuronal population. Neurotrophin-3 (NT-3), a member of the neurotrophic factor family, holds promise for the treatment of SCI. Through the specific binding to its high-affinity receptor, tropomyosin receptor kinase C (TrkC) [12], NT-3 promotes neuronal differentiation and survival and accelerates axon regeneration. Furthermore, an NT-3-enriched microenvironment may encourage the survival of grafted neurons, although this remains to be tested.

In the present study, we employed the NT-3-controlled releasing scaffold to test whether a microenvironment enriched in NT-3 could support the formation of functional NSC-derived neural network tissue (NNT) through its interaction with its receptor TrkC. We further investigated whether engineered NNT could survive in the injured spinal cord and integrate with regenerating host neural circuits. Our results showed that the sustained release of NT-3 in a biocompatible scaffold was sufficient to drive NNT formation from NSCs. The phenotypic, ultrastructural, and electrophysiological features of this NNT resembled those of mature neurons with synaptic transmission capability. Importantly, the tissue survived and integrated into the injured spinal cord, helping to improve paralyzed limb motor function in rats after SCI.

## 2. Materials and methods

### 2.1. Ethics statement

All animal experiments were conducted in accordance with Sun Yat-sen University guidelines for animal research and use.

### 2.2. Preparation of the three-dimensional (3D) culture scaffold

The 3D gelatin sponge (GS), fibroin gelatin sponge (F-GS), and NT-3/fibroin gelatin sponge (NF-GS) scaffolds were prepared as previously described [6]. Briefly, aqueous silk fibroin (SF) was extracted from silkworms (*Bombyx mori*) after washing out sericin. Recombinant NT-3 protein (0.2 µg; Sigma–Aldrich, St. Louis, MO, USA) was dissolved in 1 ml of a 1% (w/v) fibroin solution, yielding the NT-3/fibroin mixture. Finally, sterile gelatin sponges were prepared in 3-mm cylinders and soaked in 100 µl of the NT-3/fibroin mixture (for the NF-GS scaffold), 100 µl of fibroin solution (for the F-GS scaffold), or 100 µl of deionized water (for the GS scaffold). All scaffolds were freeze-dried and stored at  $-80^{\circ}\text{C}$  before use.

### 2.3. Tensile test

The thickness was assumed to be uniform along the structure. Uniaxial tensile tests were performed using a material testing machine (HYC-2011; Hongjin, Donguang, China) equipped with a 50 N load cell. Briefly, dry rectangular-shaped samples ( $30 \times 20 \times 0.2$  mm;  $n \geq 5$ ) were secured with custom clamps and stretched at a constant crosshead speed of 10 mm/min. The elastic modulus was determined according to the stress–strain curve generated. Before each test, the initial distance between the clamps was measured and samples were subjected to four initial preloading cycles to minimize the viscoelastic response of the sample during the actual tensile test. Uniaxial quasi-static tensile testing was performed at a strain rate of 2 mm/min until rupture. Force-displacement curves were recorded and engineering stress–strain values were calculated based on the initial dimensions. For each sample, the average stress magnitude was calculated for a cross-sectional area of the denticulate ligament at half-height level. The elastic modulus was determined from the slope of the linear portion of the stress–strain curve.

### 2.4. Quality filtering and analysis of the single cell atlas

To identify the receptor to which NT-3 binds to initiate robust neurogenesis, a single cell atlas was generated employing data from embryonic development. Basic quality filtering was performed according to previously described methods [13]. Doublets were detected and removed using the Python package “scrublet” (version 0.2) [14]. In total, 36,373 cells were selected for further analysis. The batch effect was eliminated using the Python package “bbknn” [15]. Dimension reduction was performed using the UMAP algorithm and clusters were identified using the Louvain clustering algorithm with the default settings from the Python package “Scanpy” (version 1.4.4) [16]. Trajectory inference and pseudotime analysis were performed according to the pipeline described in <https://github.com/julielidelle/MouseSpinalCordAtlas>.

### 2.5. Preparation of NSC culture and gene overexpression

NSCs were harvested from one-day-old GFP-transgenic (Osaka University, Osaka, Japan) or wild-type (Sun Yat-sen University, Guangzhou, China) Sprague–Dawley (SD) rats. Briefly, rats were anesthetized, the whole hippocampus was dissected, the epineurium was removed, and the tissue was dissociated in D-Hank’s solution. After centrifuging and removing the supernatant, NSCs were cultured with Dulbecco’s modified Eagle’s medium (DMEM)/F12 (DF12) supplemented with 20 µl/ml B27 (Gibco, Carlsbad, CA, USA) and 20 ng/ml basic fibroblast growth factor (Invitrogen, Carlsbad, CA, USA). Cultured cells typically grew as suspended neurospheres. Next, P0 neurospheres from GFP-transgenic SD rats were seeded into GS, F-GS, and NF-GS scaffolds (the GS+NSC, F-GS+NSC and NF-GS+NSC groups, respectively). P0 neurospheres from wild-type SD rats were infected with recombinant adenoviral (Ad) vectors expressing GFP-TrkC (Ad-GFP-TrkC) at a multiplicity of

infection (MOI) of 100 for 6 h before seeding into the above scaffolds (the GS+TrkC-NSC, F-GS+TrkC-NSC and NF-GS+TrkC-NSC groups).

## 2.6. The seeding of NSCs in the 3D engineering scaffold

A total of  $5 \times 10^5$  cells per 10  $\mu$ l of culture medium were seeded into each scaffold. To promote cell adhesion, the scaffolds with seeded cells were incubated at 37 °C for 15 min in a 24-well plate before adding 500  $\mu$ l of culture medium. The scaffolds were then further incubated for 14 days in DF12 supplemented with B27, with the culture medium being replaced every 2 days. A prolonged culture period of up to 23 days was adopted to test the action potentials and excitatory postsynaptic currents of the cells. Six groups (the GS+NSCs, GS+TrkC-NSCs, F-GS+NSCs, F-GS+TrkC-NSCs, NF-GS+NSCs and NF-GS+TrkC-NSCs groups) were tested *in vitro*.

## 2.7. The quantification of NT-3 concentration *in vitro* and *in vivo*

*In vitro*, NT-3 release from scaffolds or neural networks was detected as previously described [6]. The scaffolds or NNTs ( $n = 5$ ) were incubated in serum-free cell culture medium at 37 °C and the supernatants were collected at 1, 3, 5, 7, 14, 21, and 28 days. The concentration of NT-3 released was detected using a commercial ELISA kit (Boster, Wuhan, China). *In vivo*, ultrasonication was used to extract proteins from segments T8–T10 (mainly containing the injured/graft area) of the spinal cord of rats in the SCI, NF-GS, and neural network groups at 8 weeks after SCI ( $n = 5$ ). The NT-3 concentration was detected using an ELISA kit. Protein concentrations were standardized to total tissue weight.

## 2.8. Quantification of NSC proliferation

*In vitro*, NSCs were grown on scaffolds as mentioned above. A CCK-8 assay (Saiguoguo, Guangzhou, China) was used to test overall cell proliferation after long-term culture as well as to estimate NSC proliferation in the NF-GS+NSCs, F-GS+NSCs and GS+NSCs groups. Wells (24-well plate) without cells served as a blank control. CCK-8 (30  $\mu$ l) was added to each well (containing 300  $\mu$ l of culture medium). After 4 h of incubation at 37 °C, three 100- $\mu$ l aliquots of each sample were transferred to a 96-well plate to allow triplicate measurements. The optical density (OD) of each scaffold was measured at 450 nm. Viability was calculated based on overall cell proliferation, as follows: cell viability% = (OD test group – OD blank control group)/(OD GS+NSCs group – OD blank control group)  $\times$  100%.

## 2.9. Whole-cell patch clamp recording

To confirm mature neuronal function, action potentials and excitatory postsynaptic currents were tested using the whole-cell patch-clamp technique. An EPC Amplifier 10 (HEKA, Lamprecht, Germany) and Patchmaster software (HEKA) were used to collect the electrical signals, with a resistance of 3–5 m $\Omega$ . The external solution contained 5 mM KCl, 140 mM NaCl, 1 mM MgCl<sub>2</sub>, 2 mM CaCl<sub>2</sub>, 10 mM HEPES and 10 mM glucose (320 mOsm; pH adjusted to 7.3 with Tris-base). Electrophysiological recordings of NSC-derived neurons in the scaffolds were performed at room temperature (22–24 °C). All the drugs were applied using a microperfusion system (Langer, Baoding, China). To eliminate mobility, a nylon net was used to fix the scaffold to the object stage. Cells were tested for action potential induction and spontaneous excitatory postsynaptic current (sEPSC) generation. All data were collected and analyzed using Mini Analysis software (Synaptosoft, Decatur, GA, USA).

## 2.10. Surgery and transplantation

Rats were given a subcutaneous injection of cyclosporine A (10 mg/

kg) 3 days before surgery. Adult female SD rats (180–200 g,  $n = 76$ ) were deeply anesthetized by an intraperitoneal (i.p.) injection of 1% pentobarbital sodium (40 mg/kg). Laminectomy was performed to expose the T9 spinal segment and a 2-mm tissue segment, including the attached spinal roots, was completely removed. The NF-GS scaffold (the NF-GS group), NSCs scaffold (the NSCs group), or NF-GS+TrkC-NSCs scaffold (the NNT group) was then implanted into the gap. Surgery control rats (the SCI group) underwent the removal of the 2-mm tissue segment but not implantation. After hemostasis was achieved, the overlying musculature and skin were sequentially sutured. The animals received extensive post-operative care, including intramuscular injection of penicillin (50,000 U/kg per day) for 3 days and manual emiction three times daily, until automatic micturition function was reestablished. Cyclosporin A was administered once daily for 8 weeks.

## 2.11. Tissue processing

All the rats were deeply anesthetized with 1% pentobarbital sodium (50 mg/kg, i.p.) 8 weeks after surgery/transplantation. The rats were then intracardially perfused first with physiological saline containing heparin and 0.002% NaNO<sub>2</sub> and then with a fixative containing 4% paraformaldehyde in 0.1 M phosphate buffer (PB, pH 7.4). The tissue containing the injury/graft site of spinal cord was removed and post-fixed in fresh fixative overnight. The tissues were subsequently transferred into 30% sucrose in 0.1 M PB at 4 °C and left to sink. For immunofluorescence staining, successive segments of the spinal cord were embedded in optimal cutting temperature (OCT) compound and longitudinally sectioned into 30- $\mu$ m thick slices. For electron microscope examinations, selected segments of the spinal cord were cut into 100- $\mu$ m-thick slices using a vibratome (Microm, JENA, Germany).

## 2.12. Behavioral tests

Rats underwent the Basso–Beattie–Bresnahan (BBB) test and the inclined grid climbing test before surgery and every week after SCI. Briefly, during the BBB test, rats were allowed to freely explore an open field for 5 min to assess hindlimb locomotor frequency, joint movement range, weight bearing, and coordination. The BBB test followed a double-blind process. The 45° inclined grid climbing test was performed in the final week to qualitatively assess the accuracy of foot placement and coordination. This test could differentiate local reflex activity from voluntary movement. All the procedures were filmed by Sony HDR-PJ820E.

## 2.13. Electrophysiology

Eight weeks after surgery/transplantation, cortical motor-evoked potentials (CMEPs,  $n = 5$  per group) were recorded using a Neuro-Exam M – 800 Data Acquisition Analysis System (MEDCOM, Zhuhai, China) to assess the conductivity of the corticomotor pathway. After anesthesia (1% sodium pentobarbital, 30 mg/kg; and ketamine, 40 mg/kg) and cranial exposure, the stimulating electrode was connected to the sensorimotor cortex (SMC), and the recording electrode was connected to the sciatic nerve. CMEPs were recorded after electrical stimulation of the SMC following standard protocols. Single-pulse stimulation (50-ms duration) was applied 10 times per animal. Finally, the amplitude and latency of the CMEPs were obtained.

## 2.14. Immunofluorescence staining

After blocking with 10% goat serum, the sections and samples were incubated with primary antibodies and then with the respective secondary antibodies (Table S1). Hoechst33342 (Hoe, Invitrogen, New York, USA) was used to counterstain cell nuclei when necessary. Slides were observed under a fluorescence microscope (Leica, Wetzlar, Germany) or a confocal microscope (Carl Zeiss, JENA, Germany).

### 2.15. Western blot

Twelve rats were used to quantify the total amount of GFP protein in the spinal cord after transplantation ( $n = 6$  for each group). Equal amounts of protein (40  $\mu\text{g}$ ) were separated by 10% sodium dodecyl sulfate–polyacrylamide gel electrophoresis (SDS–PAGE) and then transferred to a polyvinylidene fluoride (PVDF) membrane. After blocking with 5% milk in Tris-buffered saline (TBS) with 0.5% Tween 20 for 1 h at room temperature, the membranes were incubated with primary antibodies (see Table S1 for detailed information) overnight at 4 °C. After washing, the membranes were treated with horseradish peroxidase (HRP)-conjugated secondary antibodies (anti-rabbit or anti-mouse, 1:5000; Jackson Immuno Research Inc., West Grove, PA, USA) for 2 h at room temperature. The bands were detected using an enhanced chemiluminescence (ECL) Western blot substrate kit (Millipore, Burlington, MA, USA). Relative band intensities were determined by densitometry using ImageJ (<https://imagej.en.softonic.com>).

### 2.16. Transmission electron microscope

Samples were washed three times with PBS, fixed in 2.5% glutaraldehyde for 60 min, and stained with 1% osmic acid for 1 h. After dehydrating through a graded ethanol series, samples were embedded in Epon overnight at 60 °C and polymerized for 48 h. Ultrathin sections were cut on an RM2065 microtome (Leica) and examined under an electron microscope (CM 10; Philips, Eindhoven, Holland).

### 2.17. Scanning electron microscope

Scanning electron microscope (SEM) was performed to observe *in vitro* cell morphology on the scaffold. After 14 days of culture, the scaffold was fixed in 4% paraformaldehyde for 15 min, washed in PBS, and then dehydrated through an ethanol series. After sputter-coating with gold, cell adherence and morphology were observed via SEM.

### 2.18. Immunoelectron microscope (IEM)

Rats were transcardially perfused first with 0.1 mol/L sodium phosphate buffer containing 187.5 units/100 ml heparin, followed by 4% paraformaldehyde, 0.1% glutaraldehyde, and 15% saturated picric acid. The spinal cord was then fixed in fresh fixative, cut into sequential 100- $\mu\text{m}$ -thick sections using a vibratome, and transferred into cryoprotectant solution containing 25% sucrose and 10% glycerol in 0.1 M PBS at 4 °C for 4 h. To improve antibody penetration, sections were treated three times with a quick freeze–thaw in liquid nitrogen and then washed with a cryoprotectant solution (2.3 M sucrose in 0.1 M PB). After blocking with 20% goat serum for 1 h, the sections were incubated with primary antibodies diluted in a 2% goat serum solution at 4 °C for 24 h. After washing, the sections were incubated with HRP mixed with 1.4-nm nanogold particles at 37 °C for 2 h, and then postfixed in 1% glutaraldehyde for 10 min. Staining was detected using the SABC-DAB Kit and the GoldEnhanced EM Plus Kit (both from NanoProbes, Yaphank, NY, USA). Finally, the sections were embedded in Epon, cut and examined by electron microscope (Philips CM 10).

### 2.19. Morphological quantification

For the quantification of percent positivity, one in every five of the whole series of sections from each scaffold was selected ( $n = 5$ ). After immunostaining with the specific markers,  $0.7 \times 0.5$  mm areas (two rostral to the injury/graft site, two caudal to the injury/graft site, and four from the injury/graft site itself) were chosen in each section. The percentage of Map2-, GFAP-, MBP- or caspase-3-positive cells in the NNT group was calculated by counting the total number of cells positive for each protein and dividing by the total number of GFP-positive cells. The percentage of ChAT-, VGluT1- or GABA-positive neurons was calculated

by counting the total number of cells positive for each factor and dividing by the total number of Map2-positive cells. The percentage of Map2- or TrkC-positive cells in the SCI and NF-GS groups was calculated by counting the total number of positive cells for these proteins and dividing by the total number of GFP-positive cells. The percentage of the postsynaptic density protein 95 (PSD95)-, synaptophysin (SYP)-, laminin (LN)-, GFP-, integrin  $\beta 1$ -, 5-hydroxytryptamine (5-HT)- or calcitonin gene-related peptide (CGRP)-positive area was calculated by counting the total density of positive areas, and dividing by the total density area of the image.

### 2.20. Statistical analysis

The data were analyzed using one-way analysis of variance (ANOVA) and expressed as means  $\pm$  standard deviation. Behavioral tests were analyzed by two-way repeated-measures ANOVA. If equal variances were found, the least-significant difference (LSD) test was applied; otherwise, the Kruskal–Wallis test followed by Dunnett's T3 post hoc test was used. The Student's *t*-test was employed for comparisons between two groups.  $P < 0.05$  was considered significant.

## 3. Results

### 3.1. Construction of a biomechanically-matched scaffold with sustained NT-3 release

To construct bioscaffolds with sustained NT-3 release and with a low swelling property that would allow subsequent cell seeding, we adopted a method previously used to produce NF-GS scaffolds [6,17]. Immunoelectron microscope (IEM) was employed to visualize the actual loading and distribution of NT-3 molecules inside the scaffolds with the aid of nanogold-conjugated secondary antibodies. The results showed that a large number of nanogold particles (green dots in Fig. 1A) were deposited on the surface of the GS. Complexity in the surface topology of the scaffold was associated with increased clustering of nanogold particles (Fig. 1B). To construct a scaffold that would be implantable in the spinal cord, the NF-GS scaffold was molded into a cylindrical shape 2 mm in length and 2 mm in diameter, and was wrapped in a tube of thin poly(lactic-co-glycolic acid) (PLGA) film (0.05 mm thick) of the same size (Fig. 1C). The scaffold (NF-GS) was then ready for *in vivo* implantation. The cumulative amount of NT-3 released from the scaffold was quantified by ELISA. The results showed that NT-3 was stably released for at least 28 days at an average of  $286.22 \pm 13.55$  pg/day (Fig. 1D and Table S2). The elastic moduli of the materials were as follows: PLGA, 281.41–576.43 MPa; GS, 336.60–535.57 kPa; and NF-GS, 92.13–287.73 kPa (Fig. 1E–G). The elastic moduli of the latter two scaffolds were similar to that of a normal spinal cord (200–600 kPa) [18], indicating that an NT-3-enriched microenvironment had been established in the GS.

### 3.2. The NT-3-enriched microenvironment promoted the survival of NSCs seeded in the scaffold

Next, NSCs derived from newborn GFP-transgenic rats were seeded into the NF-GS scaffold to investigate the biological effects of ambient NT-3 on cell survival and differentiation. To allow for sufficient reciprocal interactions between NSCs and their niche, cells were cultured in the NF-GS scaffold for 14 days. NSCs seeded into the other two types of scaffolds without NT-3 (the F-GS scaffold, which contained only fibroin; and the unmodified GS scaffold) were included as controls. Cells residing in the three scaffolds displayed similar viability, as determined by the CCK-8 assay (Fig. 1H). However, quantification of caspase-3-positive cells indicated that NSCs seeded in the NF-GS scaffold (Fig. 1I, the NF-GS+NSCs group,  $5.93 \pm 1.38\%$ ) exhibited better survival (showed reduced apoptotic cell death) relative to those seeded in the F-GS (Fig. 1J, the F-GS+NSCs group,  $10.18 \pm 0.86\%$ ) or GS (Fig. 1K,

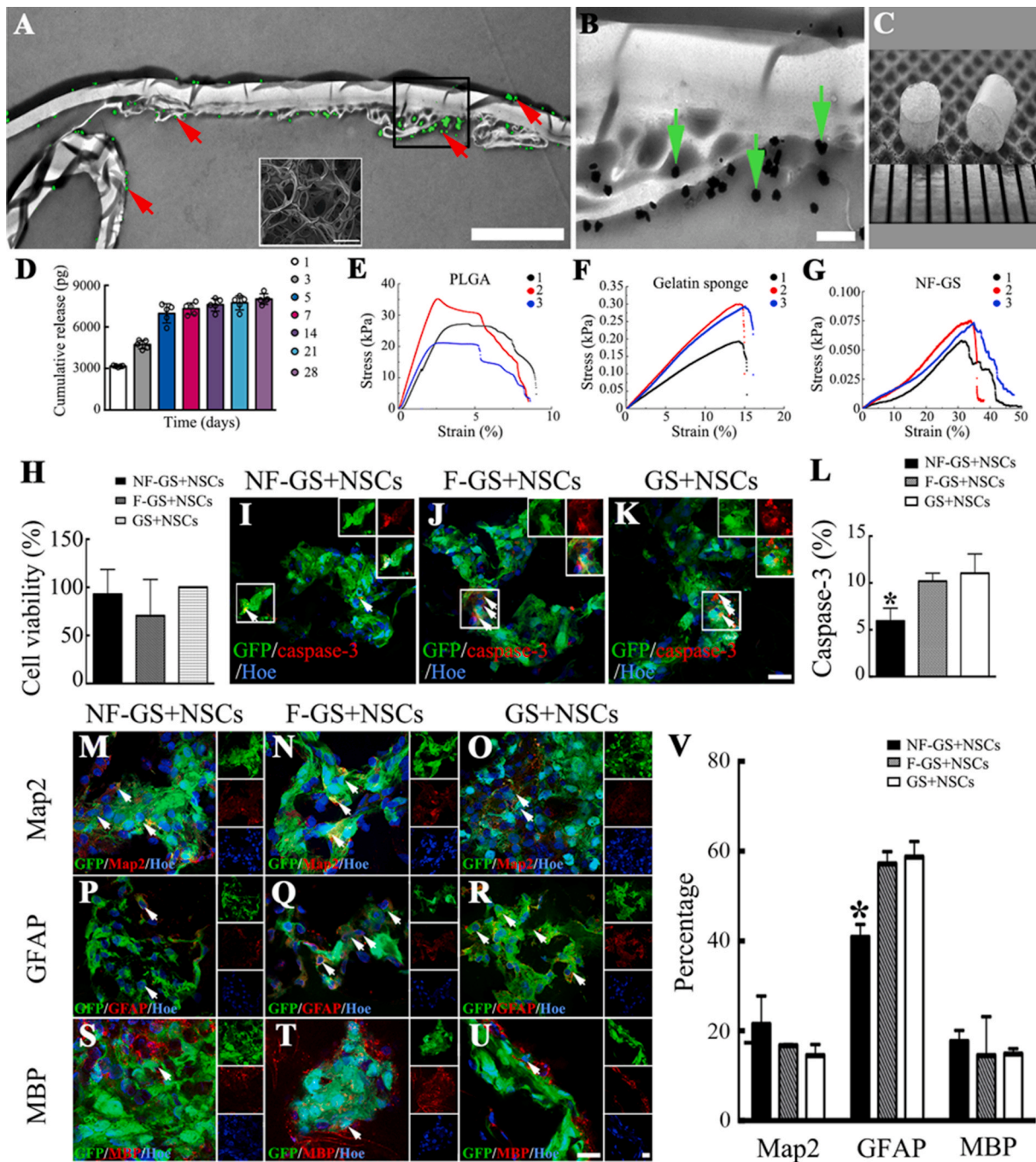


**Fig. 1.** Construction of the neurotrophin-3 (NT-3)/fibroin-releasing gelatin sponge (NF-GS) scaffold, and NT-3 enhances the survival of neural stem cells (NSCs) seeded in the scaffold. (A) Immunoelectron micrograph showing that NT-3 (probed using round, electron-dense nanogold particles; pseudocolored in green) was deposited on the surface of the gelatin sponge. The inset is a scanning electron photomicrograph showing an overview of the NF-GS scaffold. (B) Higher magnification image from (A) showing the nanogold particle-enriched area. (C) An overview of the NF-GS scaffold (3 mm in diameter and 2 mm in length). (D) Cumulative release of NT-3 from one NF-GS scaffold over 28 days *in vitro*. (E) Tensile stress-strain curves for poly(lactic-co-glycolic acid) (PLGA) from three samples (1, 2 and 3). (F) Tensile stress-strain curves for the GS scaffold from three samples (1, 2 and 3). (G) Tensile stress-strain curves for the NF-GS scaffold from three samples (1, 2 and 3). (H) A Cell Counting Kit-8 (CCK8) assay showed that cells seeded in the NF-GS scaffold, fibroin GS scaffold (F-GS), or GS scaffold exhibited similar viability. The GS + NSCs group was used as the benchmark (100%). (I)–(L) The rate of cell apoptosis was lower in the NF-GS scaffold than in the other two scaffolds. (M)–(U) After 14 days of culture, NSCs (green) differentiated into microtubule-associated protein 2 (Map2)-positive neurons, glial fibrillary acidic protein (GFAP)-positive astrocytes, and myelin basic protein (MBP)-positive oligodendrocytes in the NF-GS, F-GS and GS scaffolds. (V) Bar chart showing that there were fewer GFAP-positive cells in the NF-GS group relative to the other two groups; \* $P < 0.05$ . Hoe: Hoechst33342. Scale bars: 5  $\mu\text{m}$  in (A), 0.5  $\mu\text{m}$  in (B), 20  $\mu\text{m}$  in (I)–(K) and 25  $\mu\text{m}$  in (M)–(U). (For interpretation of the references to color in this figure legend, the reader is referred to the Web version of this article.)

the GS+NSCs group,  $11.03 \pm 2.06\%$ ) scaffolds after 14 days of culture (Fig. 1L). Immunofluorescence staining for neural lineage markers showed that NSCs seeded in all three scaffolds had neuronal, astrocytic, and oligodendrocytic differentiation potential (Fig. 1M – U).

Remarkably, NSCs residing in the NF-GS scaffold differentiated significantly less frequently into astrocytes compared with those residing in the F-GS or GS scaffolds (Fig. 1V). Taken together, these results indicated that the NF-GS scaffold supported the survival of resident NSCs

and limited their astrocytic differentiation to a greater extent than the other scaffolds. However, the NF-GS scaffold did not promote NSC-derived neuronal differentiation following 14 days of culture.

3.3. The embryonic spinal cord single cell atlas suggested that the interaction between NT-3 and TrkC boosted neurogenesis

To determine whether NSCs could be modified to express a NT-3-binding receptor and thereby enhance neuronal differentiation, we retrospectively analyzed NT-3 and its candidate gene pairs which regulate neurogenesis during normal embryonic development of the

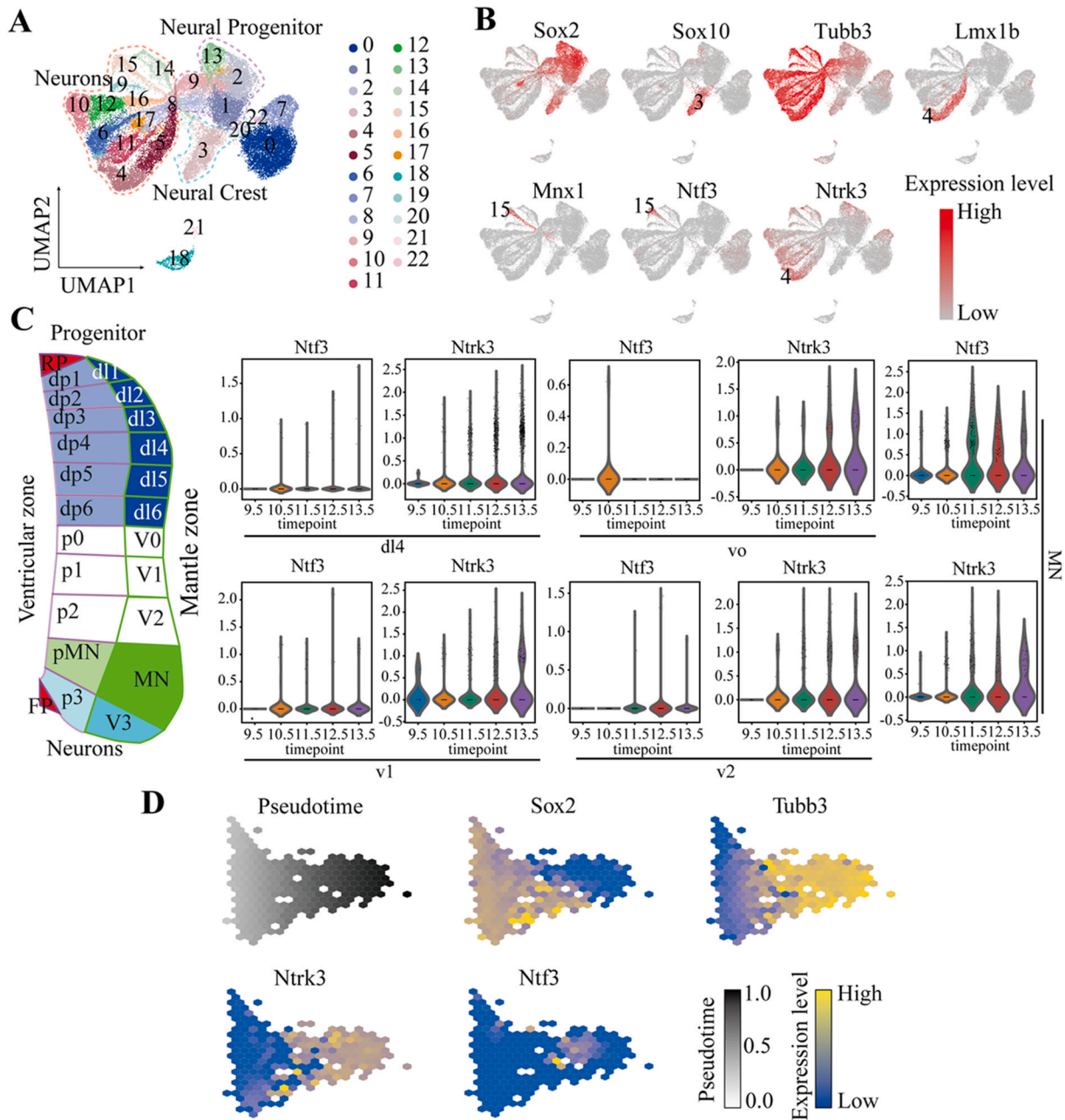


**Fig. 2.** The spatial and temporal patterns of neurotrophin-3 (*Ntf3*) and neurotrophic tyrosine kinase, receptor, type 3 (*Ntrk3*) expression during neurogenesis in the mouse embryonic spinal cord. (A) Uniform manifold approximation and projection (UMAP) plot showing all the cells of the single cell atlas. Cells are colored by their cell-type annotation and numbered according to the legend (right): 0, mesenchyme I; 1, neural progenitor I; 2, neural progenitor II; 3, neural crest; 4, neuron dl5–6 II; 5, neuron dl5–6 I; 6, neuron V0-1-V2b; 7, mesenchyme II; 8, neural progenitor III; 9, neural progenitor V; 10, neuron dl4 III; 11, neuron dl1-3-V3; 12, neuron dl4 II; 13, neural progenitor IV; 14, neural crest neurons; 15, motor neurons; 16, neuron dl4 I; 17, null neuron; 18, erythrocyte; 19, neuron V2a; 20, blood; 21, hematopoietic; and 22, myoblast. (B) UMAP plot showing the expression level of marker genes (*Sox2*, neural progenitors; *Sox10*, neural crest cells; *Tubb3*, neurons; *Lmx1b*, dl5–6 neurons; and *Mnx1*, motor neurons). The marked numbers are as in panel (A). (C) Bubble charts showing the temporal expression of *Ntf3* and *Ntrk3* in different dorsal–ventral (DV) domains during neurogenesis. The size of the circles indicates the mean expression of genes per stage and domain, and the color indicates the age of the sample. (D) Principal component analysis (PCA) projection of all neural cells, shown on a hexagonal heatmap along the pseudotime axis of neurogenesis. The hexagonal heatmaps indicate the expression pattern of *Ntrk3*, *Ntf3*, the pan-neural progenitor marker *Sox2*, and the neuronal marker, *Tubb3*. (For interpretation of the references to color in this figure legend, the reader is referred to the Web version of this article.)

mouse spinal cord using the single cell atlas. Neurotrophin-3 (*Ntf3*, encoding NT-3) has been reported to promote neuronal differentiation, neuronal survival, and axon regeneration through specific binding with its high-affinity receptor, TrkC (encoded by neurotrophic tyrosine kinase, receptor, type 3 [*Ntrk3*]). To confirm this, we downloaded the single-cell sequencing data from ArrayExpress (accession number: E-MTAB-7320) and performed quality filtering as described in the original report [13]. After reclustering the data using the uniform manifold approximation and projection (UMAP) and Leiden algorithms, we reannotated the mouse embryonic spinal cord single cell atlas (see Fig. 2A and the Materials and methods). A more comprehensive cell atlas than the one presented in the original report was mapped, allowing the developmental trajectory from neural progenitors to differentiated neurons to be determined. Intriguingly, by marking cell types with known marker genes (*Sox2*, neural progenitors; *Sox10*, neural crest cells; *Tubb3*, all neurons; *Lmx1b*, dl5–6 neurons; and *Mnx1*, motor neurons), we found that *Ntf3* was specifically expressed in motor neurons, while the gene for its receptor, *Ntrk3*, was widely expressed in almost all neurons, especially dl5–6 neurons, and even in glial progenitor cells

(Fig. 2B).

To explore the spatiotemporal expression pattern of *Ntf3* and *Ntrk3*, we divided neural progenitors and neurons into different cell populations based on the distinct domains defined in the original report, and determined the expression patterns of *Ntf3* and *Ntrk3* in the different domains and developmental stages of the mouse spinal cord. The results demonstrated that *Ntf3* was not expressed in all progenitors, being mainly expressed in motor neurons as early as embryonic day 9.5 (E9.5). In contrast, *Ntrk3* was expressed at low levels in various neural progenitors, with its expression tending to increase with developmental age from E9.5 to E13.5. On the other hand, *Ntrk3* was continuously expressed at high levels in all neurons as early as E10.5 (Fig. 2C and D). This suggested that *Ntrk3* regulates both the maturation of neural progenitor cells and their differentiation into neurons. In summary, secreted NT-3 and its receptor, TrkC, play an important role in neurogenesis in the embryonic spinal cord and promote the differentiation of neural progenitors into neurons. This suggested that the interaction between NT-3 and TrkC had the potential to promote the differentiation of NSCs into neurons and improve the therapeutic efficacy of NSC

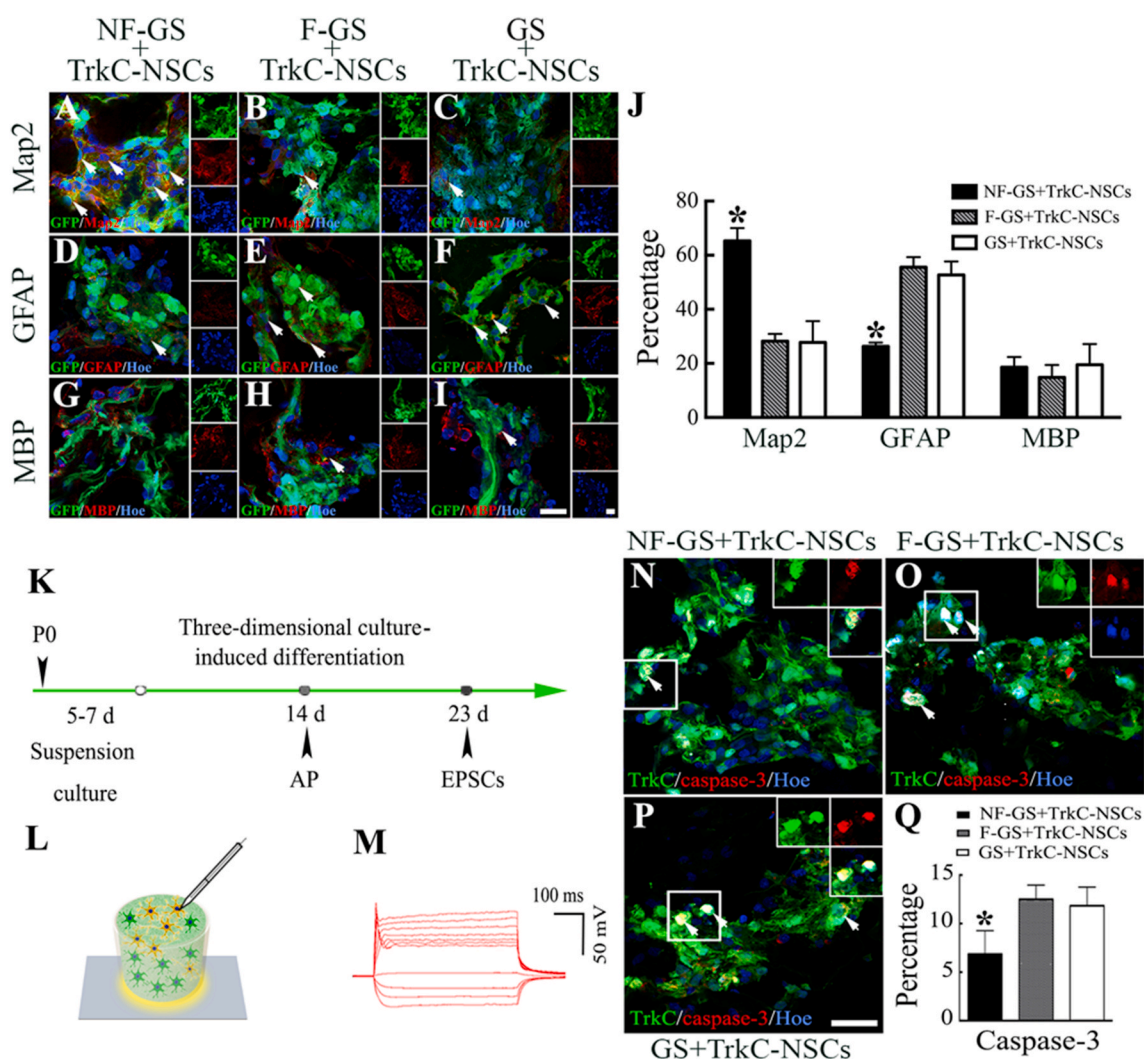


**Fig. 3.** The NF-GS scaffold promoted neuronal differentiation and the survival of seeded *tropomyosin receptor kinase C* (*TrkC*)-modified neural stem cells (NSCs) (TrkC-NSCs). (A)–(I) Green fluorescent protein (GFP)-TrkC-positive NSCs differentiated into microtubule-associated protein 2 (Map2)-positive neurons, glial fibrillary acidic protein (GFAP)-positive astrocytes, and myelin basic protein (MBP)-positive oligodendrocytes in the NF-GS, F-GS, and GS scaffolds. (J) Bar chart showing that TrkC-NSCs differentiated more frequently into Map2-positive neurons and less frequently into GFAP-positive astrocytes in the NF-GS scaffold relative to the F-GS and GS scaffolds. (K) Schematic diagram illustrating the timepoints at which action potentials (APs) or excitatory postsynaptic currents (EPSCs) were recorded from TrkC-NSC-derived neurons. (L) The patch clamp recording method. (M) APs recorded in a TrkC-NSC-derived neuron in the NF-GS scaffold. (N)–(Q) Cell apoptosis among TrkC-overexpressing cells was lower in the NF-GS group than in the F-GS or GS groups; \* $P < 0.05$ . Hoe: Hoechst33342. Scale bars: 25  $\mu\text{m}$  in (A)–(I) and 20  $\mu\text{m}$  in (N)–(P). (For interpretation of the references to color in this figure legend, the reader is referred to the Web version of this article.)

transplantation in SCI.

### 3.4. NT-3 release by the NF-GS scaffold promoted neuronal differentiation and the survival of seeded *TrkC*-NSCs

Next, we aimed to investigate whether neuronal differentiation could be significantly enhanced after seeding *TrkC*-modified NSCs into the NF-GS scaffold. For this, primary cultured NSCs were infected with an adenoviral vector carrying the *TrkC* (*TrkC*-NSCs; infection rate > 90% at a MOI of 200), and then seeded in the NF-GS scaffold. Remarkably, after 14 days of culture, the cell population immunopositive for Map2 (a marker of mature neurons) was markedly increased among the *TrkC*-NSCs seeded in the NF-GS scaffold (NF-GS+*TrkC*-NSCs group, 65.30 ± 4.74%) relative to those seeded in the F-GS (F-GS+*TrkC*-NSCs group, 28.26 ± 2.64%) or GS (GS+*TrkC*-NSCs group, 27.78 ± 7.86%) scaffolds (Fig. 3A–J). Meanwhile, the astroglial population was significantly decreased in the NF-GS+*TrkC*-NSCs group (26.32 ± 1.38%) relative to the F-GS+*TrkC*-NSCs (55.56 ± 3.76%) or GS+*TrkC*-NSCs (52.70 ± 4.98%) groups (Fig. 3A–J). Functional validation of *TrkC*-NSC-derived neurons was performed using whole-cell patch clamp recording. We adopted a previously reported methodology to record electrical signals from individual neurons residing in the scaffold *in situ* (Fig. 3K–L). After 14 days of culture in the NF-GS scaffold, *TrkC*-NSCs differentiated into neurons capable of firing action potentials (Fig. 3M), a fundamental feature of functional neurons. Action potentials (APs) were recorded in 5 out of 19 cells tested. No AP was recorded in the other groups (Fig. S1). Notably, NT-3 released from the NF-GS scaffolds promoted the survival

of *TrkC*-NSCs and derived differentiated cells after 14 days of culture, as evidenced by the lower percentage of caspase-3-immunopositive cells in the NF-GS+*TrkC*-NSC group (6.85 ± 2.41%) when compared with those of the other two groups (12.50 ± 1.46% and 11.93 ± 2.01% for the F-GS+*TrkC*-NSC and GS+*TrkC*-NSC groups, respectively, Fig. 3N–Q).

### 3.5. *TrkC*-NSC-derived neurons formed an excitatory neural network in the NF-GS scaffold

Next, we sought to determine whether *TrkC*-modified neurons in the NF-GS scaffold connected to each other to form a neural network capable of synaptic transmission. Immunofluorescence staining for SYP, a presynaptic marker, and PSD95, a postsynaptic marker, indeed showed that several *TrkC*-NSCs differentiated into neurons expressing SYP and/or PSD95 (Fig. 4A). The percentage of cells co-expressing both SYN and PSD95 was 48.90 ± 17.26%. The fluorescence intensity of both SYP and PSD95 was significantly higher in the NF-GS+*TrkC*-NSCs group (5.01 ± 0.26%, Fig. 4A and B) than in the GS+*TrkC*-NSCs group (0.63 ± 0.16%, Fig. S2 and Fig. 4B), indicating that the NT-3-enriched micro-environment encouraged the formation of synaptic connections. Transmission electron microscope validated the presence of synapses between NSC-derived neurons in the NF-GS+*TrkC*-NSCs group. There were more asymmetric than symmetric synapses, as characterized by the presence of spherical vesicles in the presynaptic component and thickened, postsynaptic densities in the postsynaptic component, suggesting that most of the synapses were likely to be excitatory (Fig. 4C–F). This assumption was supported by the fact that ChAT-positive neurons

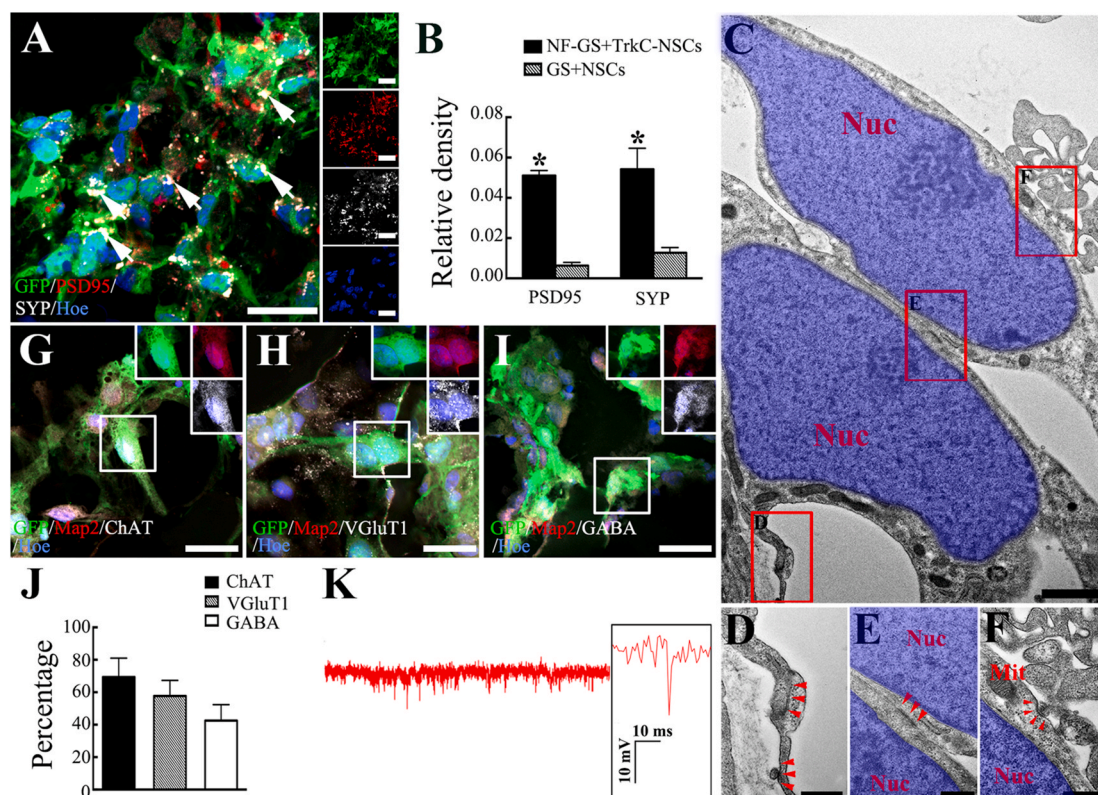


**Fig. 4.** The NF-GS scaffold supported the formation of a neural network by seeded *TrkC*-modified NSCs (*TrkC*-NSCs). (A) *TrkC*-NSCs expressed both postsynaptic density protein 95 (PSD95, red), a postsynaptic marker, and the presynaptic marker synaptophysin (SYP, white) in the NF-GS scaffold after 14 days of culture. (B) A bar chart showing that the relative fluorescence intensity of both PSD95 and SYP was significantly higher in the NF-GS+*TrkC*-NSCs group than in the GS+NSCs group. (C)–(F) TEM revealed the presence of abundant intercellular junctions between *TrkC*-NSC-derived cells (Nuc: nucleus, blue pseudocolor; Mit: mitochondria). Some intercellular junctions resembled synapse-like features. (G)–(J) *TrkC*-NSC-derived neurons expressed the cholinergic marker choline acetyltransferase (G, inset), the glutamatergic marker glutamate transporter 1 (VGluT1) (H, inset), or the GABAergic marker gamma-aminobutyric acid (GABA) (I, inset). (K) Representative excitatory postsynaptic currents (EPSCs) recorded in *TrkC*-NSC-derived neurons cultured in the NF-GS scaffolds for 23 days; \**P* < 0.05. Hoe: Hoechst33342. Scale bars: 40 μm in (A), 1 μm in (C), 200 nm in (D)–(F) and 20 μm in (G)–(I). (For interpretation of the references to color in this figure legend, the reader is referred to the Web version of this article.)

( $69.40 \pm 11.63\%$  among all the GFP-TrkC-Map2-positive cells, Fig. 4G, J) and VGlut1-immunopositive neurons ( $57.72 \pm 9.56\%$ , Fig. 4H, J) were more abundant than GABA-positive neurons ( $47.44 \pm 9.80\%$ ) in the NF-GS + TrkC-NSC group. Notably, these effects were likely promoted by the NT-3 released by the NF-GS scaffolds (Fig. 4J). Following 14–23 days of culture, the incidence of sEPSCs in TrkC-NSC-derived neurons was significantly increased (Fig. 4K), suggestive of robust excitatory signal transmission in the neural network.

### 3.6. The formation of a self-organizing engineered neural network

The GS scaffold exhibited excellent cytocompatibility with NSC-derived neural cells. Accordingly, the NF-GS scaffold provided a supportive matrix and an NT-3-enriched niche for the formation of tissue-like parenchyma. After 14 days of culture, multiple layers of highly viable neural cells had aggregated inside the NF-GS scaffold, as indicated by transmission electron microscopic observation. The neural aggregates in the scaffold possessed several key features of a neuropile, including a large number of unmyelinated axons, dendrites, and glial processes, and formed a synaptically dense region (Fig. 5A–D). Myelin sheaths were scarce and the lamellae were thin (Fig. 5E and F). Scanning electron microscope revealed that several cell processes attached to the NF-GS matrix formed network-like contacts (Fig. 5G). Such adhesion may have been the result of specific cell–matrix interactions. Indeed, immunofluorescence staining showed that NSC-derived cells deposited abundant laminin onto the NF-GS matrix after 14 days of culture. The laminin matrix secreted by NSC-derived cells may have facilitated the outgrowth of cell processes expressing integrin  $\beta 1$ , the laminin receptor

(Fig. 5H–L). Taken together, the above results indicated that the pro-neurogenic microenvironment provided by the NF-GS scaffold favored neuronal differentiation and supported the continuous maturation of TrkC-NSCs. In turn, following long-term culture, these cells modified the NF-GS matrix through the deposition of their own extracellular matrix (ECM) components, including laminin. Such a configuration enabled the *in vitro* formation of a functional entity formed from the NSC-derived neural network and the dynamic matrix, which we hereafter call the self-organized engineered neural network (sONNT).

### 3.7. NT-3 released by the NF-GS scaffold facilitated the long-term survival of grafted NNT in the injured spinal cord

We next tested whether the NT-3-enriched microenvironment provided by the NF-GS scaffold could support the long-term survival of exogenous NNT in the injured spinal cord. Two months after transplanting the NNT into the injury gap of the spinal cord segment in the NNT group, the NT-3 protein level in the grafted segment ( $140.19 \pm 8.17$  ng/g) was comparable to that in the NF-GS group (NF-GS scaffold implantation,  $151.52 \pm 8.25$  ng/g); however, it was significantly higher than that in the SCI group ( $27.59 \pm 1.87$  ng/g), as quantified by ELISA (Table S3). This suggested that an NT-3-enriched microenvironment was maintained for up to 2 months after NNT or NF-GS scaffold implantation. This trophic niche greatly promoted the long-term survival of the donor cells, as evidenced by the approximately threefold larger GFP-positive population in the NNT group relative to the NSCs group (in which NSCs were seeded in the GS scaffold before transplantation) at 8 weeks after surgery (Fig. 6A–E). Additionally, the NT-3-enriched

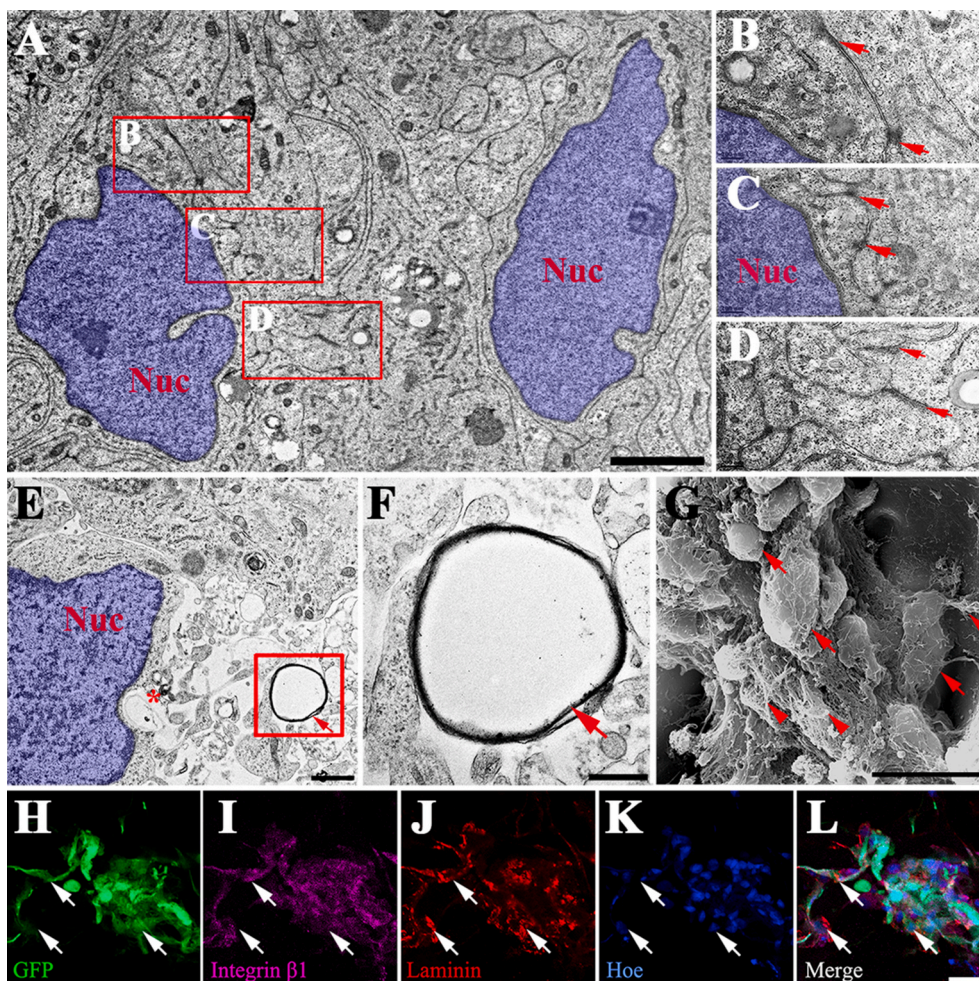


**Fig. 5.** The formation of TrkC-modified NSC-derived neural tissue in the NF-GS scaffold. (A) Transmission electron photomicrographs showing neuropil-like structures represented by synaptically-dense regions in the neural tissue (Nuc: nucleus, blue pseudocolor). (B)–(D) A large number of synapse-like structures (arrows) were apparent in the neural tissue. (E)–(F) A typical myelin sheath seen in the neural tissue. (G) Scanning electron micrograph showing that cells (arrows) attached to the surface of the scaffold, with abundant processes (arrowheads) contacting each other. (H)–(L) TrkC-NSC-derived cells expressing integrin  $\beta 1$  attached to the laminin matrix in the NF-GS scaffold. Hoe: Hoechst33342. Scale bars: 2  $\mu$ m in (A), 200 nm in (B)–(D), 20  $\mu$ m in (E), 800 nm in (F), 300 nm in (G) and 40  $\mu$ m in (H)–(L). (For interpretation of the references to color in this figure legend, the reader is referred to the Web version of this article.)

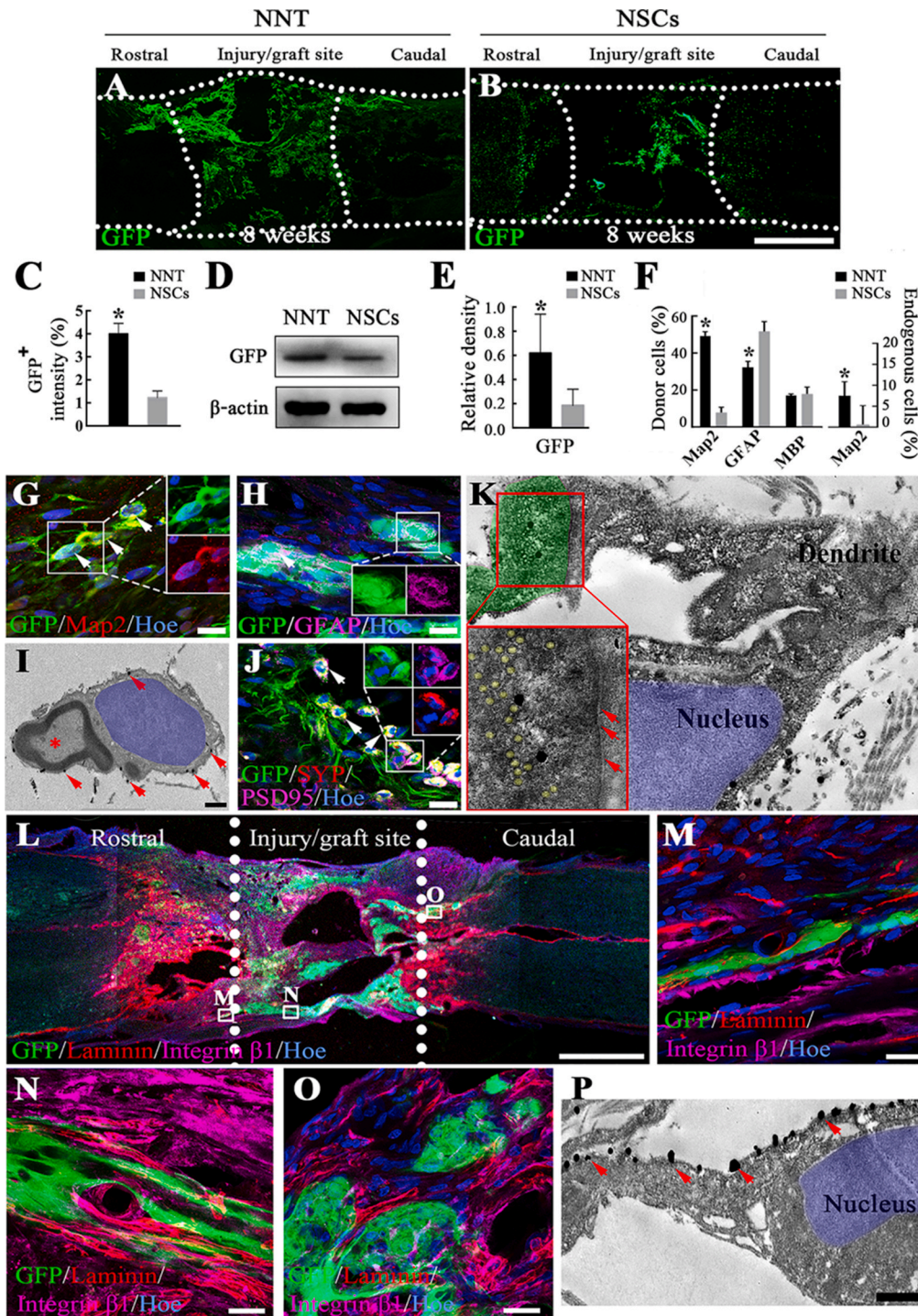


**Fig. 6.** Neural network tissue (NNT) derived from *TrkC*-modified NSCs survived in the injury/graft site of the spinal cord for 8 weeks after transplantation. (A)–(C) Surviving GFP-positive donor cells were significantly more frequently observed in the NNT group than in the NSC group (without neural network induction). (D) and (E) Western blot analysis showing the differential GFP expression between the NNT group and the NSC group. (F) A bar chart showing the maintenance of the dominant neuronal population within the NNT graft composed of donor and endogenous Map2-immunopositive neurons. (G) and (H) Representative Map2-positive donor neurons (G) and GFAP-positive donor astrocytes. (I) Transmission electron micrograph showing a donor oligodendrocyte (nanogold particle labeling, arrows; Nuc: nucleus, blue pseudocolor) forming a myelin sheath to enwrap a host nerve fiber (asterisk). (J) GFP-positive donor neurons expressing synaptophysin (SYP), a presynaptic marker, and postsynaptic density protein95 (PSD95), a postsynaptic marker. (K) Immunoelectron micrograph showing that GFP- (DAB-labeled) and TrkC- (nanogold particle-labeled) positive donor neurons (Nuc: nucleus, blue pseudocolor) formed synaptic connections (green showing presynaptic element composed of axon terminal of a neuron), with identifiable presynaptic vesicles (yellow pseudocolor) and postsynaptic densities (arrows). The inset shows a higher magnification of the synaptic structure (arrows showing synaptic cleft). (L)–(O) Significant laminin deposition was observed in the injury/graft site and the rostral and caudal areas adjacent to the injury/graft site after NNT transplantation. Some donor cells expressed integrin  $\beta$ 1. (P) Immunoelectron micrograph showing a GFP-positive donor cell (DAB-labeled) that has adhered to the linear laminin matrix (nanogold particle-labeled, arrows); \* $P < 0.05$ . Hoe: Hoechst33342. Scale bars: 1 mm in (A), (B) and (L); 20  $\mu$ m in (G), (H), (J), (M), (N) and (O); 1  $\mu$ m in (I) and (P); and 0.5  $\mu$ m in (K). (For interpretation of the references to color in this figure legend, the reader is referred to the Web version of this article.)

microenvironment supported the survival of donor neural tissue, as shown by the number of Map2-positive neurons ( $49.29 \pm 2.28\%$ ), GFAP-positive astrocytes ( $32.33 \pm 3.19\%$ ), and MBP-positive oligodendrocytes ( $17.09 \pm 0.86\%$ , Fig. 6F–I), as well as the survival rate of endogenous regenerated neurons (Fig. S3 and Fig. 6F). In particular, IEM using nanogold particles to probe for GFP revealed that donor cells formed myelin sheaths around host nerve fibers (Fig. 6I). Few donor or endogenous neurons were observed in the NSCs or SCI groups (Figs. S4A and D). However, a number of astrocytes and myelinated oligodendrocytes were distributed in the injury/graft site in the NSCs and SCI groups (Figs. S4B, C, E, F). A subset of donor cells expressing the presynaptic marker SYP or the postsynaptic marker PSD95 made contacts with each other (Fig. 6J), suggesting the formation of synapses. Indeed, synaptic structures formed between two donor neurons (using DAB-positive GFP and nanogold particles to probe for TrkC) as evidenced by IEM (Fig. 6K). Notably, the NT-3-enriched microenvironment may also have encouraged endogenous neurogenesis within the injury/graft area, as approximately  $7.48 \pm 1.28\%$  of the injury/graft area was occupied by endogenous neurons (Fig. 6F and Fig. S3). Likely due to the secreted NT-3, there were significantly more endogenous TrkC-expressing cells in the injury/graft site in the NF-GS group (NF-GS scaffold implantation) than in the SCI group (the surgery control group without scaffold implantation) (Fig. S5). A subset of TrkC-positive neurons was present in the injury/graft site in the NF-GS group, in sharp contrast to their scarcity in the injury/graft site in the SCI group (Fig. S5). Furthermore, the level of the support substrate laminin was significantly increased following the implantation of the NF-GS scaffold (Fig. S6). Integrin  $\beta 1$ -expressing donor cells within the NNT were found to aggregate in the laminin-depositing area (Fig. 6L–O). IEM showed that a GFP-positive (DAB-labeled) cell process had elongated alongside the laminin (nanogold particle labeling in Fig. 6P).

### 3.8. Grafted NNT integrated with descending 5-HT-positive or ascending CGRP-positive nerve fibers

To confirm that the grafted NNT had integrated with host neural circuits, we performed immunofluorescence staining to probe for 5-HT in nerve fibers (representing descending supraspinal tracts) and for CGRP (representing ascending sensory nerve fibers). Two months after NNT transplantation, some 5-HT-positive nerve fibers had regenerated into the center of the injury/graft site, and had made close contacts with GFP-positive donor cells (Fig. 7A–C). IEM showed that the 5-HT-positive nerve fibers (labeled with nanogold particles) made close contacts with newborn neurons in the injury/graft site (Fig. 7D and E). However, relatively few regenerating 5-HT-positive fibers had penetrated the entire injury/graft site into the area caudal to the injury/graft site. The regeneration of ascending CGRP-positive nerve fibers was more robust, as evidenced by the large number of CGRP-positive nerve fibers detected in the injury/graft site (Fig. 7F–K). A subset of CGRP-positive nerve fibers made contacts with GFP-positive donor cells located in the center of the injury/graft site. The close contacts between CGRP-positive nerve fibers and GFP-positive donor cells expressing PSD-95 may indicate synapse formation (Fig. 7L). Immunoelectron micrograph displayed that synapses had formed between a CGRP-positive nerve fiber (DAB-labeled) and a neuron in the injury/graft site (Fig. 7M, N). Immunoelectron micrograph showed a myelin sheath enwrapping a regenerated CGRP nerve fiber in the injury/graft site (Fig. 7O). Synapse-like structures were formed between CGRP-positive (DAB-labeled) nerve fibers and GFP-positive donor cells (nanogold particle labeling in Fig. 7P–R). Taken together, these findings suggested that the transplanted NNT became structurally integrated into representative host neural circuits.

### 3.9. NNT transplantation improved locomotor function

We next assessed hindlimb coordination. When rats underwent the inclined grid test, frequent plantar placement with body weight support

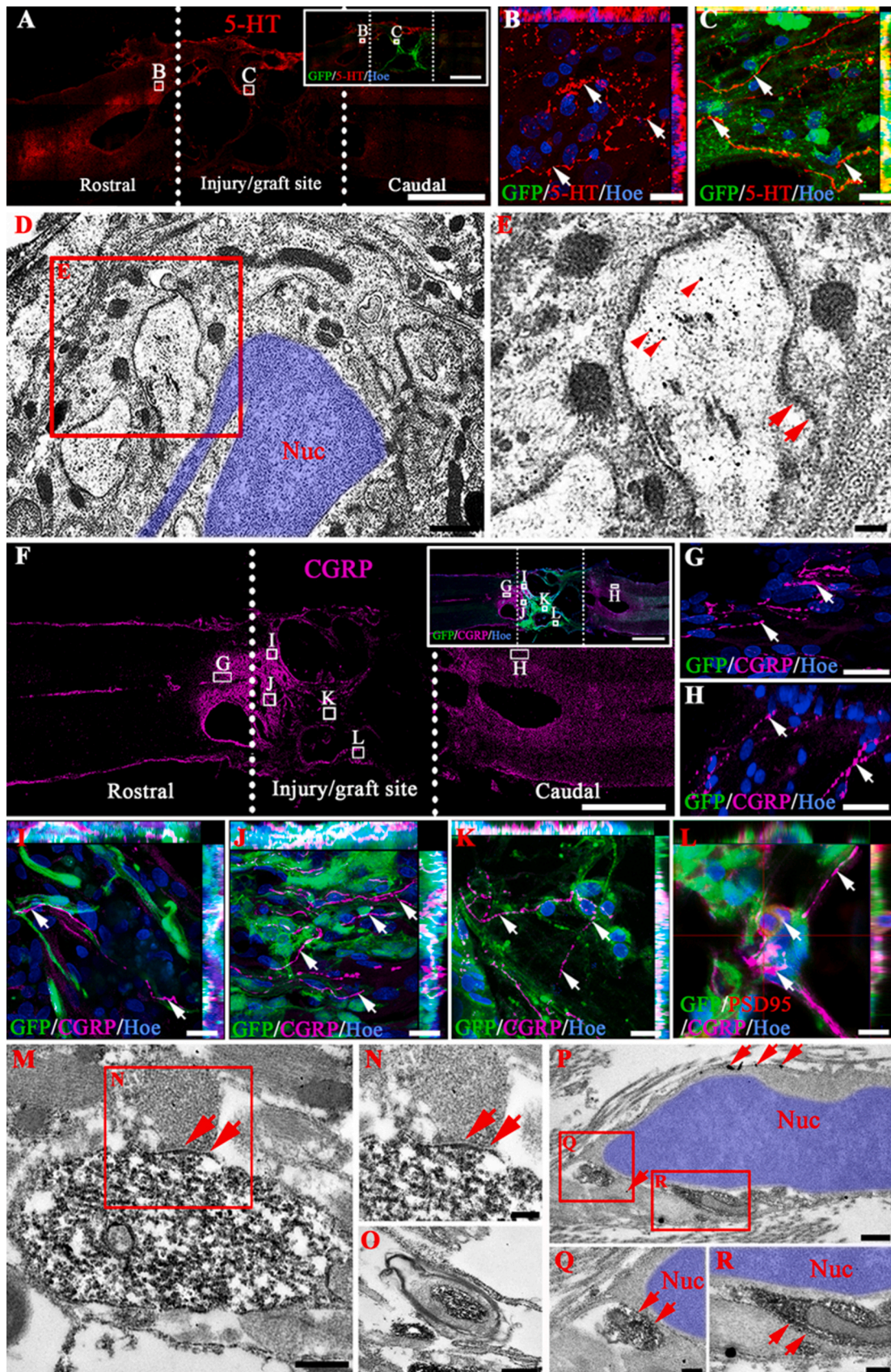
was observed only in the NNT group. In contrast, the hindlimbs of rats in the NSCs, NF-GS, and SCI groups exhibited passive movement without plantar placement on the grid during climbing (Fig. 8A). The BBB scoring scale was used to assess hindlimb motor function in rats in the open field test. Immediately after spinal cord transection, BBB scores were 0 in all the rats across all the groups, including the NNT, NSCs, NF-GS (NF-GS-implanted), and SCI (transection surgery without implantation) groups, followed by a gradual recovery in motor function within a 2-month observation period. At the end of the 2 months, the mean BBB score in the NNT group ( $7.10 \pm 0.89$ ) was significantly higher than those in the control groups (NSCs,  $4.30 \pm 0.58$ ; NF-GS,  $3.90 \pm 0.42$ ; SCI,  $2.80 \pm 0.27$ ; Fig. 8B).

Furthermore, transcranial electrophysiological recordings were performed to obtain CMEPs, which revealed the amplitude and velocity of cortical electrical signals passing to the sciatic nerve via the injury/graft site. Besides the negligible CMEP signals detected in the SCI group, CMEPs were recorded in the NNT, NSCs and NF-GS groups (Fig. 8C). Among all the groups, only the NNT group exhibited a significantly increased CMEP amplitude and a shortened CMEP latency (Fig. 8D and E). This suggested that the transplanted NNT may act as a “relay” to help rebuild ruptured neural circuits and facilitate the conduction of descending brain-derived signals across the injury/graft site of spinal cord.

## 4. Discussion

Over recent years, accumulating evidence in both canines [17] and nonhuman primates [4] has indicated that a single neural trophic factor, NT-3, can be a potent inducer of a pro-regenerative microenvironment that favors endogenous repair after severe SCI. However, several technical hurdles must be overcome before NT-3-producing neuronal grafts with augmented efficacy in treating SCI can be generated. Among these, the maturation of donor neurons and their integration with the host neural tissue are of particular concern. In the current study, we first employed bioinformatics-based screening to identify a neurotrophic factor suitable for use in the construction of a bioactive scaffold to repair SCI. Subsequently, we devised a ligand–receptor responsive approach to promote the neuronal differentiation of TrkC-NSCs that exhibited excellent viability and functional maturity in the NT-3-releasing GS scaffold. With sufficient culture and induction time, NSC-derived neurons made synaptic connections with each other to form NNT. Aided by the persistent release of NT-3, the donor NSC-derived NNT survived for up to 8 weeks in the hostile post-SCI microenvironment and integrated with regenerating host neural circuits, leading to a significant recovery of motor function in paralyzed limbs. These results suggested that employing a single neural trophic factor represents a feasible and effective regimen for use in engineering neural grafts that have the potential to repair SCI.

After traumatic SCI, particularly that which results in a large tissue defect, the harsh post-injury microenvironment (primarily caused by chronic inflammation) poses great challenges to the survival of spared and regenerating neural tissue, as well as that of grafted tissue [19]. The promotion of a pro-regenerative microenvironment is a key strategy for overcoming this drawback. Studies have shown that NT-3 plays an important role in inhibiting neuronal death in the central nervous system [20,21]. Consequently, it should be possible to create an NT-3-enriched microenvironment that limits the death of spared or grafted neurons. For example, early studies using an intrathecal delivery method (via bolus injection or an osmotic minipump) to supply NT-3 to the injured spinal cord resulted in robust protection of endangered local neurons [22]. In this study, an NT-3-enriched microenvironment was established through the grafting of a GS scaffold exhibiting sustained NT-3 release and excellent biocompatibility into the injured area of the spinal cord. Grafting of the GS scaffold with persistent NT-3 delivery has been shown to promote axon regeneration, attenuate inflammation, and induce cell migration in rodent and canine SCI models [6]. Such an



(caption on next page)

**Fig. 7.** The donor neural network integrated with the descending and ascending neural circuits of the host. (A)–(C) Descending 5-HT-positive nerve fibers regenerated into the area rostral to the injury/graft site (B) and into the center of the injury/graft site (C), making contacts with GFP-positive donor cells within the neural network graft. (D) and (E) An immunoelectron micrograph showing that a 5-HT-positive (nanogold particle-labeled, arrowheads) nerve fiber formed contacts (arrows) with a neuron (Nuc: nucleus, blue pseudocolor) from the injury/grate site. (F)–(K) CGRP-positive nerve fibers regenerated into areas rostral (G) and caudal (H) to the injury/graft site, and some made close contacts with GFP-labeled donor cells within the neural network graft (I–K). (L) A PSD95-positive donor neuron contacting a CGRP-positive nerve fiber (arrows). (M) and (N) Immunoelectron micrograph showing the formation of synapses between a CGRP-positive nerve fiber (DAB-labeled) and an endogenous cell in the injury/graft site. (O) Immunoelectron micrograph showing a myelin sheath enwrapping a regenerated CGRP-positive fiber in the injury/graft site. (P)–(R) Immunoelectron micrograph showing the formation of synapse-like structures between two CGRP-positive nerve fibers (DAB-labeled) and a GFP-positive donor cell (nanogold particle-labeled). Hoe: Hoechst33342. Scale bars: 1 mm in (A) and (F); 20  $\mu$ m in (B), (C) and (G)–(L); 0.5  $\mu$ m in (D), (M), (O) and (P); 200 nm in (E), (N), (Q) and (R). (For interpretation of the references to color in this figure legend, the reader is referred to the Web version of this article.)

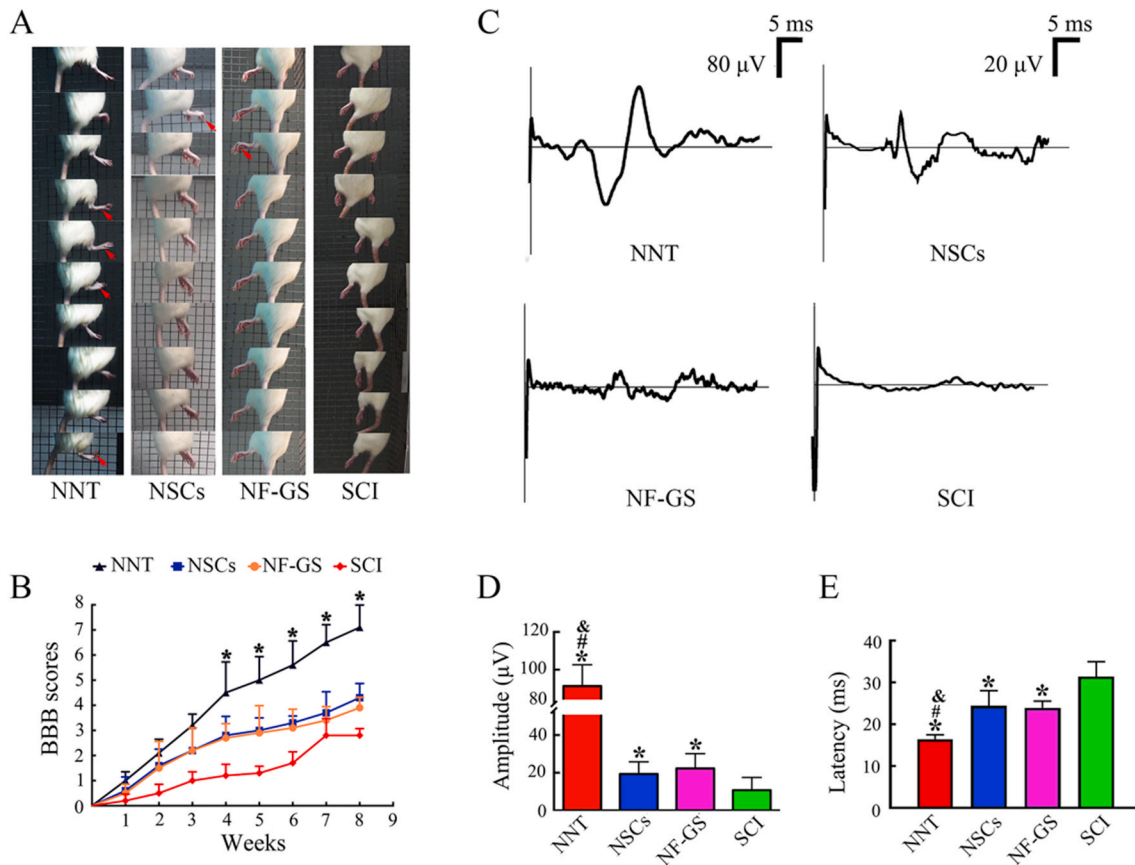


**Fig. 8.** Grafted neural network tissue (NNT) improved motor function recovery and electrophysiological activity. (A) Frequent plantar placement with body weight support was observed only in the NNT group in the inclined grid test. (B) Basso-Beattie-Bresnahan (BBB) scoring showing that there was a significant improvement in hindlimb motor function after NNT transplantation. (C) Representative recorded cortical motor evoked potentials (CMEPs). (D) and (E) Rats in the NNT group had larger CMEP amplitudes and shorter CMEP latencies compared with those of rats in the control groups. \* $P < 0.05$ , vs. the spinal cord injury group; # $P < 0.05$ , vs. the NF-GS group; & $P < 0.05$ , vs. the NSCs group.

NT-3-enriched microenvironment supports the long-term survival of NSC-derived neurons both *in vitro* (14 days) and *in vivo* (up to 8 weeks in the spinal cord). Meanwhile, studies have shown that the application of exogenous NT-3 can initiate endogenous neurogenesis immediately following SCI [4,6], presumably through the direct activation of ependymal NSCs present in the spinal cord [23], thereby compensating for tissue loss. In this study, endogenous neural cells were also observed following implantation of the NF-GS scaffold. We have previously shown that NT-3 functions as a chemokine, directly recruiting TrkC-expressing stem cells both *in vitro* and in the injured spinal cord [24]. As observed in the current study, an NT-3-enriched microenvironment may allow the continuous differentiation of endogenous NSCs into neurons and the survival of newly born TrkC-expressing neurons in the injury/graft area of spinal cord. Taken together, these results suggested that the modified microenvironment established by the grafted NT-3-releasing scaffold in the injured area of the spinal cord may have supported the survival of

both exogenous neurons and endogenous newborn neurons. This could result in a significant increase in the neuronal population in the injury/graft site, which may eventually contribute to the structural repair of sensorimotor pathways.

Studies have shown that replenishing the neuronal population, but not the astrocytic population, is correlated with neural function recovery following SCI [25,26]. However, it remains challenging to sufficiently increase the rate of neuronal differentiation from grafted or endogenous NSCs [25] to override the gliogenic cues within the predominantly gliogenic milieu at the site of injury. For example, neurogenin-2, a basic helix-loop-helix transcription factor that controls neuronal fate decisions [27], contributes to an unexpectedly low level of neuronal differentiation among NSCs grafted in the injured spinal cord [28]. Manipulation of the epigenetic status of NSCs can result in more effective neuronal differentiation. For example, the administration of valproic acid (VPA), a known antiepileptic and histone deacetylase

inhibitor, during NSC transplantation into the spinal cord significantly increased the neuronal differentiation rate of donor NSCs from a negligible level to approximately 20% over 5 weeks [29]. However, such neuronal commitment may still not be enough, given that the authors reported that over 60% of the donor cells retained an astroglial phenotype. This highlights the importance of creating a neurogenic microenvironment, rather than genetically or epigenetically modulating the donor cells. Indeed, drastic modification of the microenvironment by the administration of a battery of trophic factors, including brain-derived neurotrophic factor (BDNF), NT-3, glial cell-derived neurotrophic factor (GDNF), epidermal growth factor (EGF), basic fibroblast growth factor (bFGF), acidic fibroblast growth factor (aFGF), hepatocyte growth factor (HGF), insulin-like growth factor 1 (IGF-1), platelet-derived growth factor (PDGF), vascular endothelial growth factor (VEGF), and a calpain inhibitor MDL28170, resulted in high rates of neuronal differentiation among human neural progenitor cells (approximately 57%) grafted into the injured spinal cord of rodents [30] or nonhuman primates [31]. Similarly, we previously showed that most NSCs differentiate into neurons when co-cultured with Schwann cells (SCs), which can secrete a variety of trophic factors [32]. In particular, NT-3-modified SCs can increase the neuronal differentiation rate of TrkC overexpressing NSCs by up to 60%, both *in vitro* and in the spinal cord [33]. In our study, retrospective analysis of a single cell atlas generated with data from the embryonic spinal cord indicated that NT-3 and its receptor, TrkC, play an important role in neurogenesis and neuronal maturation in the developing spinal cord. Using this information, we achieved a proof-of-concept, namely, that a single trophic factor, NT-3, can promote the neuronal differentiation of TrkC-overexpressing NSCs to an adequate level. Within the NT-3-enriched microenvironment of the 3D culture system, TrkC overexpressing NSCs differentiated into neurons with mature phenotypes and electrophysiological function. Importantly, with continuing culture, exogenous NT-3, together with other secreted factors and ECM proteins (such as laminin) derived from the differentiating cells, created a unique niche that encouraged the formation of a tissue-like assembly, functioned as a neural network, and was capable of generating spontaneous postsynaptic currents. NT-3, in particular, may play an instrumental role in enhancing synapse formation and transsynaptic activity [34], presumably via TrkC-mediated PI3K/AKT/mTOR and PI3K/AKT/CREB pathways [33]. Therefore, in this study, we called this engineered construct a sONNT. The autonomy of the structural and functional entity is believed to have resulted from the initiation and continuous replenishment of the ambient NT-3 concentration, as well as from the dynamic integration between stem cells and the ECM deposited on the GS scaffold.

NSCs adhere poorly to a regular matrix. To improve NSC seeding in 3D engineering scaffolds, we follow certain procedures that we have developed based on several years of experience. 1.) The prepared scaffolds must have sufficient porosity (100–500  $\mu\text{m}$ ) to allow NSC spheres to fill the pores. 2.) A cylindrical poly(lactic-co-glycolic acid) (PLGA) film was coated on the surface of the gelatin sponge to restrict the flow of liquid in the scaffold, which can reduce the diffusion of cells at the beginning of planting. 3.) After the cells were seeded on the material, they were precultured in the incubator for 25 min, and the medium was added after the cells had stably adhered. 4.) Silk fibroin coating provides a certain degree of ion affinity, and it can better adhere to the wall under the effect of adherent culture medium. Robert Langer's group used polylysine (PLL) to modify the surface of the PLGA scaffold, allowing easier NSC seeding [35], while Tuszynski et al. used methacrylate gelatin (GelMa) gel to load cells into biomimetic 3D-printed scaffolds for spinal cord injury repair [18]. A different group developed linear ordered collagen scaffolds, which provided a surface for cell growth and differentiation, and enhanced the repair of nerve injury in rats [36]. N-cadherin has been reported to regulate the mechanical adhesion of scaffolds and promote the adhesion of NPCs on collagen scaffolds [37]. This observation indicates that the adhesion of NSCs to 3D materials can be effectively improved by altering the surface properties of scaffold

materials and increasing the ionic affinity between cells and scaffolds. On this basis, our neuroengineering strategy recapitulates the principle of “fourth dimension” (4D) biology which emphasizes the “time” factor for functional tissue construction [38,39]. This “4D” culture process presents a tangible methodology for predicting cell state and fate *in vivo*.

Through our tissue engineering approach, we generated a graftable NNT suitable for repairing SCI with large tissue defects. However, whether grafted NNT can contribute to the recovery of neural function depends on the extent of graft–host integration. In this study, we first demonstrated the viability and phenotypic maintenance of donor neurons. For functional recovery, the re-establishment of neuronal connectivity in the injured area is fundamental [26]. Using IEM, we showed that the donor neurons formed synaptic connections with each other or with regenerating host nerve fibers in the injury/graft site. We suggest that three primary elements were likely responsible for the restoration of neuronal connectivity in the injured site. 1.) The pro-regeneration microenvironment generated by the sustained release of NT-3 was chemotactic to regenerating nerve fibers. Exogenous NT-3 not only supported neuronal differentiation and survival, but also increased the regeneration of brain-derived descending nerve bundles [40] and ascending sensory nerve bundles [41] (assessed using 5-HT-expressing and CGRP-expressing nerve fibers, respectively, in this study). 2.) The permissive ECM deposited in the NNT facilitated the migration of regenerating tissue and the outgrowth of regenerating nerve fibers. Modulating the expression of permissive ECM proteins, such as laminin, may override the inhibitory effect of chondroitin sulfate proteoglycan, the major component of the glial scar, on axon regeneration [42]. Indeed, our work suggested that laminin was abundantly deposited during the formation of the NNT. Laminin molecules may provide the substrate for the regenerating tissue [5,43], while surviving donor neurons provide targets for the regenerating host nerve fibers. Loss of tropism by the target neuron results in axon degeneration [44]. 3.) The NSC-derived NNT in a NT-3-releasing scaffold was devised to serve as a “neuronal relay” to repair the SCI. In this scenario, exogenous or endogenous neurons relay neural signals in the injury site without long-distance regeneration of the descending motor tracts, as long as they form contacts with the relay neurons [45]. As descending 5-HT nerve fibers of the raphespinal tract (RpST) are reportedly relevant for locomotor recovery [46,47]. In this study, IEM result shows that 5-HT-positive nerve fibers formed contacts with the transplanted neurons, and electrophysiological readouts of CMEPs suggests that brain-derived neural signals were relayed to the caudal spinal cord and then to the lower limbs through the transplanted cells, as evidenced by improved motor function. Therefore, our neuroengineering strategy that resulted in a mixed population of neurons may provide target-derived tropism for regenerating nerve fibers. In particular, postsynaptic TrkC molecules overexpressed in donor neurons may bind presynaptic protein tyrosine phosphatase sigma (PTP $\sigma$ ), leading to synaptic adhesion and stabilization [48]. Our strategy resulted in an engineered NNT capable of reconnecting ascending and descending neural signals and supporting neural transmission, thereby helping to repair the sensorimotor pathway.

## 5. Conclusions

Based on the mechanism underlying neural induction in the embryonic spinal cord, in this study, we utilized a specific ligand–receptor interaction to construct NNT *in vitro* by culturing TrkC-overexpressing NSCs in a scaffold exhibiting sustained NT-3 release. The engineered NNT was self-organized within the NT-3-enriched microenvironment and showed typical neural excitability. When grafted into the injured spinal cord, the NNT survived and integrated with host neural circuits, and supported neural transmission, thereby helping to restore motor function. These results constitute a proof-of-concept, namely, that by binding to its receptor (TrkC), a regimen comprising a single neural trophic factor (NT-3) may be enough to support neurogenesis with

mature neuronal function and efficacy in treating SCI. Based on this design, the interactions between various neurotrophic ligands and their corresponding receptors can be used to construct graftable NNT suitable for different therapeutic purposes.

#### Declaration of interests

The authors declare no conflict of interest.

#### CRediT authorship contribution statement

**Ge Li:** Formal analysis, Writing – original draft, Methodology. **Bao Zhang:** Formal analysis, Writing – original draft, Methodology. **Jia-hui Sun:** Methodology, Data curation. **Li-yang Shi:** Methodology, Data curation. **Meng-yao Huang:** Methodology, Data curation. **Li-jun Huang:** Methodology, Data curation. **Zi-jing Lin:** Methodology, Data curation. **Qiong-yu Lin:** Methodology, Data curation. **Bi-qin Lai:** Formal analysis, Writing – original draft. **Yuan-huan Ma:** Formal analysis, Writing – original draft. **Bin Jiang:** Formal analysis, Writing – original draft. **Ying Ding:** Formal analysis, Writing – original draft. **Hong-bo Zhang:** Formal analysis, Writing – original draft. **Miao-xin Li:** Formal analysis, Writing – original draft. **Ping Zhu:** Formal analysis, Writing – original draft. **Ya-qiong Wang:** Methodology, Data curation. **Xiang Zeng:** Writing – original draft, Supervision. **Yuan-shan Zeng:** Writing – original draft, Supervision.

#### Declaration of competing interest

The authors declare that they have no known competing financial interests or personal relationships that could have appeared to influence the work reported in this paper.

#### Acknowledgements

This work was supported by the Chinese National Natural Science Foundation of China (81891003), the National Key R&D Program of China (2017YFA0104700) and the 111 Project for Academic Exchange Program (B13037) to Y.S. Zeng; the Foundation of Guangdong Province (2017B020210012) to Y.S. Zeng and X. Zeng; the Co-innovation Foundation of Guangzhou City (201704020221) to Y.S. Zeng, X. Zeng, and G. Li; and the Start-up Foundation of Guangdong Province (Grant No. 2018A030310113) to G. Li.

#### Appendix A. Supplementary data

Supplementary data to this article can be found online at <https://doi.org/10.1016/j.bioactmat.2021.03.036>.

#### References

- G. Courtine, M.V. Sofroniew, Spinal cord repair: advances in biology and technology, *Nat. Med.* 25 (6) (2019) 898–908.
- A. Alizadeh, S.M. Dyck, S. Karimi-Abdolrezaee, Traumatic spinal cord injury: an overview of pathophysiology, models and acute injury mechanisms, *Front. Neurol.* 10 (2019) 282.
- Y.D. Teng, Functional multipotency of stem cells and recovery neurobiology of injured spinal cords, *Cell Transplant.* 28 (4) (2019) 451–459.
- J.S. Rao, C. Zhao, A. Zhang, H. Duan, P. Hao, R.H. Wei, J. Shang, W. Zhao, Z. Liu, J. Yu, K.S. Fan, Z. Tian, Q. He, W. Song, Z. Yang, Y.E. Sun, X. Li, NT3-chitosan enables de novo regeneration and functional recovery in monkeys after spinal cord injury, *Proc. Natl. Acad. Sci. U. S. A.* 115 (24) (2018) E5595–E5604.
- M.A. Anderson, T.M. O’Shea, J.E. Burda, Y. Ao, S.L. Barlaty, A.M. Bernstein, J. H. Kim, N.D. James, A. Rogers, B. Kato, A.L. Wollenberg, R. Kawaguchi, G. Coppola, C. Wang, T.J. Deming, Z. He, G. Courtine, M.V. Sofroniew, Required growth facilitators propel axon regeneration across complete spinal cord injury, *Nature* 561 (7723) (2018) 396–400.
- G. Li, M.T. Che, K. Zhang, L.N. Qin, Y.T. Zhang, R.Q. Chen, L.M. Rong, S. Liu, Y. Ding, H.Y. Shen, S.M. Long, J.L. Wu, E.A. Ling, Y.S. Zeng, Graft of the NT-3 persistent delivery gelatin sponge scaffold promotes axon regeneration, attenuates inflammation, and induces cell migration in rat and canine with spinal cord injury, *Biomaterials* 83 (2016) 233–248.
- C.G. Becker, T. Becker, J.P. Hugnot, The spinal ependymal zone as a source of endogenous repair cells across vertebrates, *Prog. Neurobiol.* 170 (2018) 67–80.
- P. Lu, Y.Z. Wang, L. Graham, K. McHale, M.Y. Gao, D. Wu, J. Brock, A. Blesch, E. S. Rosenzweig, L.A. Havton, B.H. Zheng, J.M. Conner, M. Marsala, M.H. Tuszynski, Long-distance growth and connectivity of neural stem cells after severe spinal cord injury, *Cell* 150 (6) (2012) 1264–1273.
- E.S. Rosenzweig, J.H. Brock, P. Lu, H. Kumamaru, E.A. Salegio, K. Kadoya, J. L. Weber, J.J. Liang, R. Moseanko, S. Hawbecker, J.R. Huie, L.A. Havton, Y.S. Nout-Lomas, A.R. Ferguson, M.S. Beattie, J.C. Bresnahan, M.H. Tuszynski, Restorative effects of human neural stem cell grafts on the primate spinal cord, *Nat. Med.* 24 (4) (2018) 484–490.
- J.N. Dulin, P. Lu, Bridging the injured spinal cord with neural stem cells, *Neural Regen. Res.* 9 (3) (2014) 229–231.
- P. Lu, L. Graham, Y. Wang, D. Wu, M. Tuszynski, Promotion of survival and differentiation of neural stem cells with fibrin and growth factor cocktails after severe spinal cord injury, *JoVE* 89 (2014), e50641.
- H. Edalat, Z. Hajebrahimi, V. Pirhajati, M. Tavallaei, M. Movahedin, S.J. Mowla, Exogenous expression of nt-3 and TrkC genes in bone marrow stromal cells elevated the survival rate of the cells in the course of neural differentiation, *Cell. Mol. Neurobiol.* 37 (7) (2017) 1187–1194.
- J. Delile, T. Rayon, M. Melchionda, A. Edwards, J. Briscoe, A. Sagner, Single cell transcriptomics reveals spatial and temporal dynamics of gene expression in the developing mouse spinal cord, *Development* 146 (12) (2019) dev173807.
- S.L. Wolock, R. Lopez, A.M. Klein, Scrublet: computational identification of cell doublets in single-cell transcriptomic data, *Cell Syst.* 8 (4) (2019) 281–291 e9.
- K. Polanski, J.E. Park, M.D. Young, Z. Miao, K.B. Meyer, S.A. Teichmann, BBKNN: fast batch Alignment of single cell transcriptomes, *Bioinformatics* 36 (3) (2020) 964–965.
- F.A. Wolf, P. Angerer, F.J. Theis, SCANPY: large-scale single-cell gene expression data analysis, *Genome Biol.* 19 (1) (2018) 15.
- G. Li, M.T. Che, X. Zeng, X.C. Qiu, B. Feng, B.Q. Lai, H.Y. Shen, E.A. Ling, Y.S. Zeng, Neurotrophin-3 released from implant of tissue-engineered fibroin scaffolds inhibits inflammation, enhances nerve fiber regeneration, and improves motor function in canine spinal cord injury, *J. Biomed. Mater. Res.* 106 (8) (2018) 2158–2170.
- J. Koffler, W. Zhu, X. Qu, O. Platoshy, J.N. Dulin, J. Brock, L. Graham, P. Lu, J. Sakamoto, M. Marsala, S. Chen, M.H. Tuszynski, Biomimetic 3D-printed scaffolds for spinal cord injury repair, *Nat. Med.* 25 (2) (2019) 263–269.
- H. Katoh, K. Yokota, M.G. Fehlings, Regeneration of spinal cord connectivity through stem cell transplantation and biomaterial scaffolds, *Front. Cell. Neurosci.* 13 (2019) 248.
- A. Galan, S. Jmaeff, P.F. Barcelona, F. Brahim, M.V. Sarunic, H.U. Saragovi, In retinitis pigmentosa TrkC.T1-dependent vectorial Erk activity upregulates glial TNF-alpha, causing selective neuronal death, *Cell Death Dis.* 8 (12) (2017) 3222.
- B. Ye, Q. Wang, H. Hu, Y. Shen, C. Fan, P. Chen, Y. Ma, H. Wu, M. Xiang, Restoring autophagic flux attenuates cochlear spiral ganglion neuron degeneration by promoting TFEB nuclear translocation via inhibiting MTOR, *Autophagy* 15 (6) (2019) 998–1016.
- M.M. Lavail, S. Nishikawa, J.L. Duncan, H. Yang, M.T. Matthes, D. Yasumura, D. Vollrath, P.A. Overbeek, J.D. Ash, M.L. Robinson, Sustained delivery of NT-3 from lens fiber cells in transgenic mice reveals specificity of neuroprotection in retinal degenerations, *J. Comp. Neurol.* 511 (6) (2008) 724–735.
- Y. Ke, L. Chi, R. Xu, C. Luo, D. Gozal, R. Liu, Early response of endogenous adult neural progenitor cells to acute spinal cord injury in mice, *Stem Cell.* 24 (4) (2006) 1011–1019.
- Y.F. Chen, X. Zeng, K. Zhang, B.Q. Lai, E.A. Ling, Y.S. Zeng, Neurotrophin-3 stimulates migration of mesenchymal stem cells overexpressing TrkC, *Curr. Med. Chem.* 20 (24) (2013) 3022–3033.
- F. Barnabe-Heider, J. Frisen, Stem cells for spinal cord repair, *Cell Stem Cell* 3 (1) (2008) 16–24.
- P. Assinck, G.J. Duncan, B.J. Hilton, J.R. Pleml, W. Tetzlaff, Cell transplantation therapy for spinal cord injury, *Nat. Neurosci.* 20 (5) (2017) 637–647.
- M. Nieto, C. Schuurmans, O. Britz, F. Guillemot, Neural bHLH genes control the neuronal versus glial fate decision in cortical progenitors, *Neuron* 29 (2) (2001) 401–413.
- C.P. Hofstetter, N.A. Holmstrom, J.A. Lilja, P. Schweinhardt, J. Hao, C. Spenger, Z. Wiesenfeld-Hallin, S.N. Kurpad, J. Frisen, L. Olson, Allodynia limits the usefulness of intraspinal neural stem cell grafts; directed differentiation improves outcome, *Nat. Neurosci.* 8 (3) (2005) 346–353.
- M. Abematsu, K. Tsujimura, M. Yamano, M. Saito, K. Kohno, J. Kohyama, M. Namihira, S. Komiya, K. Nakashima, Neurons derived from transplanted neural stem cells restore disrupted neuronal circuitry in a mouse model of spinal cord injury, *J. Clin. Invest.* 120 (9) (2010) 3255–3266.
- P. Lu, Y. Wang, L. Graham, K. McHale, M. Gao, D. Wu, J. Brock, A. Blesch, E. S. Rosenzweig, L.A. Havton, B. Zheng, J.M. Conner, M. Marsala, M.H. Tuszynski, Long-distance growth and connectivity of neural stem cells after severe spinal cord injury, *Cell* 150 (6) (2012) 1264–1273.
- K. Kadoya, P. Lu, K. Nguyen, C. Lee-Kubli, H. Kumamaru, L. Yao, J. Knackert, G. Poplawski, J.N. Dulin, H. Strobl, Y. Takashima, J. Biane, J. Conner, S.C. Zhang, M.H. Tuszynski, Spinal cord reconstitution with homologous neural grafts enables robust corticospinal regeneration, *Nat. Med.* 22 (5) (2016) 479–487.
- M. Fallon, P. Tadi, *Histology, Schwann Cells, StatPearls*, 2020. Treasure Island (FL).
- B.Q. Lai, M.T. Che, B.L. Du, X. Zeng, Y.H. Ma, B. Feng, X.C. Qiu, K. Zhang, S. Liu, H. Y. Shen, J.L. Wu, E.A. Ling, Y.S. Zeng, Transplantation of tissue engineering neural

- network and formation of neuronal relay into the transected rat spinal cord, *Biomaterials* 109 (2016) 40–54.
- [34] Q. Li, M. Chen, C. Zhang, T. Lu, S. Min, S. Li, Opposite roles of NT-3 and BDNF in synaptic remodeling of the inner ear induced by electrical stimulation, *Cell. Mol. Neurobiol.* (2020), <https://doi.org/10.1007/s10571-020-00935-x>.
- [35] Y.D. Teng, E.B. Lavik, X. Qu, K.I. Park, J. Ourednik, D. Zurakowski, R. Langer, E. Y. Snyder, Functional recovery following traumatic spinal cord injury mediated by a unique polymer scaffold seeded with neural stem cells, *Proc. Natl. Acad. Sci. U. S. A.* 99 (5) (2002) 3024–3029.
- [36] Y. Zou, D. Ma, H. Shen, Y. Zhao, B. Xu, Y. Fan, Z. Sun, B. Chen, W. Xue, Y. Shi, Z. Xiao, R. Gu, J. Dai, Aligned collagen scaffold combination with human spinal cord-derived neural stem cells to improve spinal cord injury repair, *Biomater. Sci.* 8 (18) (2020) 5145–5156.
- [37] W. Liu, B. Xu, W. Xue, B. Yang, Y. Fan, B. Chen, Z. Xiao, X. Xue, Z. Sun, M. Shu, Q. Zhang, Y. Shi, Y. Zhao, J. Dai, A functional scaffold to promote the migration and neuronal differentiation of neural stem/progenitor cells for spinal cord injury repair, *Biomaterials* 243 (2020) 119941.
- [38] M.W. Tibbitt, K.S. Anseth, Dynamic microenvironments: the fourth dimension, *Sci. Transl. Med.* 4 (160) (2012) 160ps24.
- [39] Y. Setty, I.R. Cohen, Y. Dor, D. Harel, Four-dimensional realistic modeling of pancreatic organogenesis, *Proc. Natl. Acad. Sci. U. S. A.* 105 (51) (2008) 20374–20379.
- [40] V.S. Boyce, L.M. Mendell, Neurotrophins and spinal circuit function, *Front. Neural Circ.* 8 (2014) 59.
- [41] B.N. Lilley, Y.A. Pan, J.R. Sanes, SAD kinases sculpt axonal arbors of sensory neurons through long- and short-term responses to neurotrophin signals, *Neuron* 79 (1) (2013) 39–53.
- [42] M.V. Sofroniew, Dissecting spinal cord regeneration, *Nature* 557 (7705) (2018) 343–350.
- [43] S.J. Taylor, J.W. McDonald 3rd, S.E. Sakiyama-Elbert, Controlled release of neurotrophin-3 from fibrin gels for spinal cord injury, *J. Contr. Release* 98 (2) (2004) 281–294.
- [44] M. Kerschensteiner, M.E. Schwab, J.W. Lichtman, T. Misgeld, In vivo imaging of axonal degeneration and regeneration in the injured spinal cord, *Nat. Med.* 11 (5) (2005) 572–577.
- [45] J.F. Bonner, O. Steward, Repair of spinal cord injury with neuronal relays: from fetal grafts to neural stem cells, *Brain Res.* 1619 (2015) 115–123.
- [46] C.S. Siegel, K.L. Fink, S.M. Strittmatter, W.B. Cafferty, Plasticity of intact rubral projections mediates spontaneous recovery of function after corticospinal tract injury, *J. Neurosci.* 35 (4) (2015) 1443–1457.
- [47] M. Leibinger, C. Zeitler, P. Gobrecht, A. Andreadaki, G. Gisselmann, D. Fischer, Transneuronal delivery of hyper-interleukin-6 enables functional recovery after severe spinal cord injury in mice, *Nat. Commun.* 12 (1) (2021) 391.
- [48] H. Takahashi, P. Arstikaitis, T. Prasad, T.E. Bartlett, Y.T. Wang, T.H. Murphy, A. M. Craig, Postsynaptic TrkC and presynaptic PTPsigma function as a bidirectional excitatory synaptic organizing complex, *Neuron* 69 (2) (2011) 287–303.